The Pennsylvania State University

The Graduate School

Department of Mechanical and Nuclear Engineering

EFFECTS OF CARBON MATERIALS AS ADDITIVES ON THE COMBUSTION BEHAVIOR OF DOUBLE-BASE PROPELLANT

A Thesis in

Mechanical Engineering

by

Skylar Schirtzinger

Submitted in Partial Fulfillment
of the Requirements
for the Degree of

Master of Science

August 2017

The thesis of Skylar Schirtzinger was reviewed and approved* by the following:

Richard Yetter
Professor of Mechanical Engineering
Director of the High Pressure Combustion Lab
Thesis Advisor

Stefan Thynell
Professor of Mechanical Engineering

Karen Thole
Department Head of Mechanical and Nuclear Engineering
Distinguished Professor of Mechanical Engineering

*Signatures are on file in the Graduate School

ABSTRACT

Carbon materials such as graphite, graphene and functionalized graphene sheets have been shown to have enhanced effects on the burning/combustion of propellants. The increased availability of specialized carbon materials leads to greater interest in understanding how these materials affect propellant performance. In this investigation, five types of carbon materials (graphite, graphene, graphene oxide (GO), reduced graphene oxide (rGO), and carboxyl functionalized graphene sheets) were mixed with the double-base propellant (~58% NC, 40% NG) at concentrations of 0.25, 0.50, 0.75, and 1.00wt%. The effects of these additive materials and concentrations on the propellant properties, including burning rate, density and thermal decomposition were observed. A lab-scale procedure was established to produce the propellant material in the form of solid strands, which allowed for control of sample composition and testing. Propellant samples were characterized using optical strand burning measurements, and thermogravimetric analysis (TGA).

It is shown that 0.50wt% GOb exhibits statistically significant increase (approximately 1.19 times) in linear burning rate compared to the control double-base propellant with no additive. Normalizing the linear burning rate data by density for a mass burning rate revealed that 0.50wt% and 1.00wt% rGO exhibit statistically significant increase (approximately 1.11 and 1.14 time, respectively) in gas production compared to the control. The 0.75wt% and 1.00wt% graphite propellant mixtures exhibit statistically significant decrease (approximately 0.89 and 0.87 times, respectively) in the rate of gas production compared to the control. DSC-TGA data indicates that the additive materials used do not lead to more sensitive or less thermally stable propellant admixtures. Evaluation of the TGA data does indicate that 0.50wt% rGO exhibit enhanced thermal decomposition and heat release compared to the baseline propellant.

Graphene oxide, at a concentration of 0.50wt%, consistently exhibits enhancements to the combustion behavior of the base propellant. The results achieved in this investigation show that, overall, inexpensive, commercially available, carbon additives can be used as a controllable variable to tailor the performance of a double-base propellant to obtain desired characteristics.

TABLE OF CONTENTS

List of Figures

LIST OF TABLES

Nomenclature

Abbreviations

ASTM	American Section of the Internation Association for Testing Materials
BAE/RFAAP	BAE Systems at Radford Army Ammunition Plan
BSE	Back Scattered Electron
CEA	Chemical Equilibrium Analysis
COOH	Carboxyl
DAQ	Data Acquisition system
DB	Double base
DSC	Differential Scanning Calorimetry
FGS	Functionalized Graphene Sheets
GO	Graphene Oxide
GOa	Graphene Oxide produced by Graphene Labs Inc.
GOb	Graphene Oxide produced by Garmor Tech Inc.
KHPCL	Kenneth K. Kuo High Pressure Combustion Lab
MCL	Material Characterization Lab
NATO	North Atlantic Treaty Organization
NC	Nitrocellulose
NG	Nitroglycerine
NIST	National Institute for Standards and Technology
rGO	Reduced Graphene Oxide
STANAG	Standardization Agreement
SEM	Scanning Electron Microscope
TGA	Thermogravimetric Analysis

Equation Variables

F_v	Propellant Impetus (J/g)
G	Grubbs Test outlier criteria
m	Mass (g)
M_w	Molecular Weigth (g/mol)
Q	Dixon Q test oulier criteria
Ru	Universal Gas Constante (8.314 J/mol*K)

T	Temperature (units specified when used)
T_v	Adiabatic Flame Temperature (K)
t	Student-t value
V	Volume (cm^3)
Y	Mass fraction
α	Confidence level
Δ	Change/difference
δ	Modified Thompson-Tau Test outlier criteria
ρ	Density (g/cm^3)

Subscripts

DB	Property relating to Double Base propellant
additive	Property relating to an additive material
mix	Property relating to a mixture of the Double Base propellant and additive material

ACKNOWLEDGEMENTS

This thesis is the culmination of a solid two years of research and investigation. Having now completed this thesis, it is amazing to look back and see how much I did not know, across the board. After many good classes with great professors, trial and error, self-discovery, mentoring and literature review, I now feel I know marginally more than at the start. The choice to pursue a Master's of Science in Mechanical Engineering, focusing on the Thermal Science, was because the field interests me to no end, and the lessons learned in undergraduate studies only revealed there was far more to learn and appreciate about this field. Going through the program and research showed me that there are far more doors to open and explore. This journey could not have been undertaken and finished without the help, support and guidance of many groups and individuals.

I cannot express my full gratitude enough to the vast and invaluable assistance of Dr. Eric Boyer. He has been a wonderful 'boss', mentor and friend throughout my time at the Kenneth K. Kuo High Pressure Combustion Lab (KHCPL). His depth of knowledge and experience provided guidance into developing testing procedures and creating fundamental questions about data that would lead better understanding the behaviors and relationships in the system. Dr. Boyer's attitude for achieving accountable and responsible results in a practical and realistic manner has shaped me to a better researcher and technical communicator. I value the lessons and skills gleaned from him during my time working in the lab, and look forward to apply them in future hobbies and careers.

The rest of the faculty, staff and students at the KHPCL have all assisted in the researching and writing of this thesis. Dr. Andrew Cortopassi is the reason I was first hired as an undergraduate assistant to the lab and continued onwards to my own projects. His experience and previous work with data analysis and software control with experimental systems and data made

data processing and material production possible. Dr. Cortopassi and Dr. Boyer created an environment in the lab that was challenging and engaging, while still being real and practical. I feel far more prepared for the unknown (relative to my experience) challenges upon entry into the 'real world'. Best of luck and health to him and his family.

The works and expertise of the other staff and faculty associated with the KHPCL, including Dr. Terry Connel, Dr. Grant Risha, and Dr. Jeff Moore, have also been of great help. During the design and development phase for this investigation, their previous work and experience helped identify and fix reoccurring issues with testing procedures and data analysis.

Much the actual experimentation could not have been completed in a timely manner if it was not for the assistance of every student involved in the lab, including: Mike Vamos, Evan Kerr, Evan Fisher, Eric Yang, Chris Burner, Connor Carr and Stephen Tomaszewiski. They have been indispensable in working through hundreds of experimental test runs, processing and extruding test material and analyzing the data. I appreciate the help, work, and laughs from my time with everybody in the lab, both past and present. My best wishes to all of them, their families and careers.

I would like to thank my thesis and academic advisor, Dr. Richard Yetter. His insistence in understanding the fundamentals of any system provided direction about what questions to ask and data to collect to understand the implications of achieved results.

Much of the designed processes and equipment as achieved with collaboration with research partners NextGen Aeronautics, RxFF Consulting and BAE Systems and Radford Army Ammunition Plant, and research sponsor: United States Army at Picatinny Arsenal. The specialized insight into propellant behavior and production, and molecular dynamic simulation were the foundation of some of the processes and conclusions of this thesis. Continuing this work forward with these groups will be very fruitful from an academic and experience point of view.

This work would not be possible without the opportunities and experiences gained thanks to the Pennsylvania State University College of Mechanical and Nuclear Engineering. The six years I have spent at this institution have been some of the greatest in my life. I feel well prepared with the lessons and experienced from the classes and programs that were available to take on and succeed the majority of challenges I will face in future projects and careers.

I am forever grateful for the support of all varieties provided by my family throughout the entirety of my life and particularly during my academic career. My parents nurtured in me a drive to discover and understand the world around me, and to think about and investigate what I do not yet know or understand. They have been my greatest allies and most enduring fans. I will spend the rest of my life attempting to repay them for the enormous investments in time, money, effort, and love they have given to me.

To my sisters: Salina, we are related. Hi Sierra.

There is no way I can encapsulate and express the support and joy I have gotten from innumerable friends and acquaintances. They have helped me de-stress during some of the tougher times. They have provided new means of looking at a problem and communicating my thoughts. Many of them have taken a supreme and personal interest into my wellbeing. I thank this innumerable mass for letting me be me, and keeping and stoking the fire to explore further.

Chapter 1

Introduction

Since the discovery of graphene in 2004[1], the material has been heralded and popularized by many as a super material. Not only for its favorable thermal and electrical conductivities, as well as its mechanical strength, but also for the vast array of fields and applications that this relatively simple material and its derivatives can be utilized. Research into medical technologies[2] and electronics[3] have yielded products and systems that have brought great prosperity and progress. The following is an investigation to the utilization of graphene and graphene derivatives in combustion.

Graphene is a single atom thick layer of covalently bonded carbon atoms. The repeating hexagonal pattern of carbon atoms is considered a two dimensional (2D) material. The planar structure, single and double covalent bonds, and the electron affinity of carbon atoms contribute to incredible electrical, thermal and mechanical properties.[1] The magnitude of some of these properties are compared to other materials in Table 1.

Table 1: Comparison of Graphene properties to other materials

Material	Thermal Conductivity (W/m·K)	Electrical Resistivity (ohm·cm)	Tensile Strength (MPa)
Graphene	600 [4]	10^{-6} [1]	130,000 [5]
Copper[6]	398	$1.7*10^{-6}$	210
Steel (AISI 1212)[6]	51.9	$1.74*10^{-5}$	540

Graphene and its derivatives are known to have very high thermal conductivities by both theoretical and experimental[4] investigation. By homogenously mixing particles within a propellant, the additive could work to increase the bulk thermal conductivity of the mixture. Increasing the thermal conductivity for a combustion system (a propellant for example) allows for

heat from the flame zone to penetrate further into the propellant, and bring it to ignition temperature faster.[7]

Addition of carbon-rich graphene particles can increase the opacity and absorptivity of the surface and flame zone, potentially increasing the radiation heat feedback and energy delivered to the burning surface. Carbon powders have been shown to be great absorbers in the middle and near infrared ranges.[8] This suggests that the thermal radiation from the combustion could be more effectively absorbed as sensible energy, increasing the depth of the inner pre-heat zone of the propellant, similar to the effects of increasing thermal conductivity. Additionally, carbon additives within the flame would work to keep the radiative energy within the flame zone via absorption rather than radiative loss.

Carbon additives have also been shown to have catalytic effect on decomposition of intermediate species reactions that may affect energy release rate.[9] The relatively large specific surface area of particles and the high electron mobility of carbon nano-materials[10] allows the additives to serve as staging sights for charge and species transfer during chemical decomposition. In terms of fuels[11] and propellants[12], this behavior can lead to an increase in performance. Sabourin's work with functionalized graphene sheets in liquid nitromethane raised questions if similar catalytic behavior could be seen with other nitro ester compound solid propellants, such as nitrocellulose.

A readily utilized composite of nitro ester propellants is double base propellant. Double base propellants are composed of nitrocellulose (NC) and nitroglycerin (NG).[13] The relative concentration of NC and NG, and the addition of stabilizing agents leads to a large array of types of double base propellants. These propellants are readily utilized for applications of artillery propellant, firearm-reloading charges, and rockets.[14] The frequent and diverse uses of these propellants make them subjects for investigation for performance enhancement or control.

The promising aspects and research regarding graphene materials as combustion catalysts, as mentioned above, and the importance and usefulness of double-base propellants is the inciting interest to this investigation. The following chapters, results and discussions will look at the changes of performance characteristics, such as burning rate, decomposition, density, and thermal stability, of a representative double base propellant when mixed with carbon materials at various concentrations. Observing these changes will provide insight on if and how these additives can be used as a controllable parameter to tailor the performance of propellant mixtures. The potential to enhance or inhibit combustion allows for the design of charges that could increase range, accuracy or power for projectile systems. Enhancement to thermal stability would provide for safer transport, handling, and storage of propellant mixtures. The introduction of relatively low cost material to achieve optimized characteristics could present itself as a significant and effective cost saving measure.

Chapter 2

Material Selection

Additive Material

The increased interest and usage of graphene across many fields, as previously mentioned, has led to great expansion of the graphene market. A preliminary market search to identify products and availability of materials uncovered over 40 individual graphene manufacturers or providers across the globe. This market surge has led to lower cost of graphene materials as well as a plethora of graphene derivatives. For focused and meaningful research into the effect of these materials on the burning rate of a double-base propellant, it is necessary to select only a few additive materials.

The initial down selection process was achieved by only considering American manufactures or providers. Selecting only domestic suppliers is mostly driven by request from the research sponsors. Domestic suppliers typically have lower cost and faster shipping as well as simplifies purchasing orders. Eliminating foreign providers from the market search also eliminated several specialized functionalized graphene sheets such as metal-doped graphene. Much of these products were also limited in availability and quite expensive, and would not have been considered for purchase.

With the initial identification of the various manufacturers and suppliers of graphitic materials worldwide, further investigation allowed for filtering providers and products most likely of interest to this research. This investigation evaluated what types of functionalization a provider had available and whether or not that the product had potential for catalytic activity with propellants. From these notes and further considerations regarding provider nationality, product

availability and cost for both small and larger scale mixing, three types of functionalization were selected as having greatest potential for catalytic activity with the double base propellant formulation. The additive materials selected, the manufacturer, and some product properties (particle size and specific area) as specified by the manufacturer are listed in Table 2.

Table 2: Selected Additive Materials for Investigation

Material	Manufacturer	Particle Size (µm, Lateral)	Specific Area (m^2/g)
Graphite	Asbury	<44 (MIL-G-155A Grade 4)	235-265
Graphene	XG Science	5	120-150
Graphene oxide (GOa)	Graphene Labs	0.5-5	'as high as' 833
Graphene oxide (GOb)	Garmor	0.5 (90% <800nm)	220-240
Reduced Graphene Oxide (rGO)	Cheap Tubes Inc.	0.3-0.8	350
Carboxyl FGS (COOH)	Graphene Labs	0.3-5	20
DB Propellant	BAE Systems at RFAAP	~58% NC, 40%NG + Additives	

Graphite

Graphite is one of the most common forms of carbon utilized in industry and manufacturing. The large usage makes this material relatively abundant and inexpensive. This material is a crystalline matrix of graphene sheets, and is in many cases the base material in the production of graphene materials. Graphite will serve as the additive baseline for comparison for burning rate behavior. As previously mentioned, an increase in material thermal conductivity or absorptivity can work to increase propellant burning rate or rate of decomposition. Using graphite will give an indication if the graphene and functionalized graphene materials are exhibiting catalytic activity or not.

Graphene

Graphene with no additives will serve as another base of comparison for the functionalized graphene materials. The superior thermal and electrical conductivity as well as surface area of graphene flakes present their own opportunities for catalytic activity with the double-base propellant. 'Neat' graphene flakes will allow for a better understanding of how graphene properties affect combustion without the addition of other functionalized group.

Graphene Oxide (GO)

Graphene oxide (GO) is a functionalized graphene sheet (FGS) in which oxide groups are bound to a graphene sheet, an illustration of this can be seen in Figure 1. GO is usually produced as a byproduct or intermediate step in the production of non-functionalized graphene sheets. Graphene is typically produced by the Hummers and Offeman oxidation method[16], which works to separate sheets of graphene in a stacked graphite configuration. This method uses an acid (permanganate or sulfuric) to open the graphite matrix and cause deformation in the sheet layer or open valence bonding sight. Hydrogen peroxide in the solution then works to attach oxide groups to the activation sights created by the acid bath, resulting in a GO flake. The change in sheet morphology and chemical structure prevents agglomeration back into a graphite matrix.

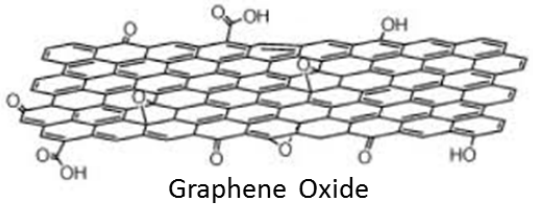

Figure 1: Illustration[16] of a sheet of Graphene Oxide

This process makes GO more readily available and less expensive compared to other functionalized graphene products. The abundance of oxide groups allows this material to undergo

reduction by means of thermal or chemical processes. ‘GO experiences significant decomposition at mild temperature; recommended for lower temperature environments’.[16] If too effective at catalyzing NC and/or NG decomposition, GO could compromise long-term storage stability or make the mixture too sensitive for safe handling.

As can be seen in Table 2, two different supplies of were used in this investigation. Initially, the supply graphene oxide from Graphene Laboratory (GOa) was purchased to serve as the GO additive. During the preliminary mixing and burning tests, the vast majority (~75%) of these propellant mixtures yielded unusable test data, frequently exhibiting signs of internal void formation greater than that experienced by other materials. After some investigation (discussed in a later section), this was shown to be due in part to very large particles size and poor distribution within the propellant. When this supply of material was consumed, a new provider of GO, Garmor (GOb), was selected. This material is proven to be much finer and led to higher quality propellant strands with usable and reliable data. Results of tests examined and discussed in this thesis are based on propellant admixtures containing GOb.

Reduced GO (rGO)

Reduced graphene oxide (rGO), like GO materials, are graphene sheets functionalized with oxide groups, and is a byproduct for the production of graphene sheets. In an attempt to recover GO flakes to a more pristine graphene sheet, the flakes are reduced to shed some of the oxide groups, as depicted in Figure 2. This process leads to both structural functionalized sites (voids) as well as oxygen groups in central and edge locations on the graphene sheet.

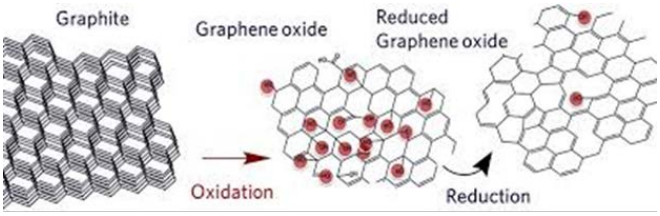

Figure 2: Illustration[17] of production of reduced graphene oxide

Voids provide a mechanism to regulate radical pools during reaction, which may in turn become new functional sites. The presence of the oxide groups may also exhibit similar behaviors as the GO but to a smaller effect. rGO has been shown to increase burning rate and decrease pressure sensitivity of nitromethane experimentally[12] and in molecular dynamics simulations[18].

Carboxyl Functionalized Graphene Sheet (FGS)

The previous four materials are relatively standard across a large number of carbon material suppliers, which was a driving consideration for their selection. A plethora of other FGS materials is also available throughout the market. It is of interest to this investigation if one of the more specialized functionalization would have a greater influence on the combustion of DB propellants. As stated before, selection was driven by cost and availability; the selection of a specialized FGS was done with considerations of how that functional group may participate in the combustion cycle.

Carboxyl groups have been shown to form as a functional group on graphene and detach as part of the cyclic catalytic reaction for nitromethane decomposition.[9] Initial carboxyl functionality could therefore potentially "jump-start" a catalytic cycle or increase the frequency of those potential cycles.

No Additive

As this investigation requires a considerable amount of material preparation to add material to the double base material, and create test samples in a usable format (geometry and consistency), it is inevitable that the utilized procedures will affect the performance of baseline propellant. As such, it is necessary to subject samples of the double-base propellant with no additive material to the same sample preparation procedures to understand and directly compare aspects of combustion behavior.

Propellant

Double base (DB) propellants are a homogenous propellant consisting of nitrocellulose (NC) and nitroglycerin (NG). For this investigation, a composition of approximately 57.7% NC, 40% NG, 0.75% ethyl centralite, and 1.50% potassium nitrate, known as M9,[19] was used as a representative DB material. The potassium nitrate in the propellant acts as a flash suppressor for artillery applications and has little effect on the burning rate of the material.[20]

A stock supply of the DB propellant solid strands was available in on-site magazines from an earlier fundamental research project. This formulation is typically manufactured and utilized in a flake form. The solid strand form is less standard in terms of the propellant usage; however, it will give insight into some of the basic characteristics and properties through using a more standard means of testing and observation.

It is important to recognize that relative to other DB propellants, the formulation used in this investigation burns faster and hotter, which may affect or even mask any enhancement contributions provided by the additive materials. Alternatively, any significant changes in the

behavior of this formulation due to the presence of an additive may be strong indication that similar results can be achieved with slower and cooler burning DB propellants.

Thermodynamic Performance

The DB propellant utilized in this investigation is inherently a fuel-rich system. Adding any amount of carbon material, itself a fuel, is unlikely to lead to an increase in the energy release from the propellant combustion. To get a better estimate of the impact that additive materials and concentration may have on the energy output of the propellant, constant volume thermodynamic equilibrium calculations were performed. These calculations will yield theoretical values of the adiabatic flame temperature and the propellant impetus.

The constant volume, adiabatic flame temperature, T_v, is the maximum attainable temperature of a system when allowed to run to complete combustion with no heat or work removed. Propellant impetus, F_v, is a measure of the maximum amount of work that can be done from a unit mass of propellant[21], and is calculated using Equation 1; where R_u is the universal gas constant and M_w is the molecular weight of the product mixture.

$$F_v = \frac{R_u T_v}{M_w} = \left[\frac{J}{g}\right] \quad (1)$$

These calculations will not give any indication of potential catalytic activity, but only a thermodynamic analysis of the system. As mentioned previously, it is not expected that these additive materials will increase the energetic output of the propellant. As such, it is expected with the addition of more carbon material the adiabatic flame temperature and propellant impetus will decrease.

The performed calculations were achieved utilizing the NASA-Glenn Chemical Equilibrium Analysis (CEA2) program, which is a publicly available and frequently utilized

program for thermodynamic reaction calculations. Each of the additive materials at each of the weight concentrations to be tested were run at a constant density condition of 0.2g/cm^3. This value is a standard characteristic loading density for performance calculations involving gun propellants and powders[22,23]. The problem setup variables, values of relative concentrations, and the names, formation energies and compositions of the reactant species are listed in Appendix A.

The values of the elemental composition and heat of formation for NC[24] and NG[25] were obtained through available literature. The values of the elemental composition and heat of formation of the additive materials, except for graphite, were calculated and provided by RxFF Consulting utilizing the reactive force field method of molecular dynamics. RxFF Consulting has worked in parallel with this investigation to perform molecular dynamic simulations of the propellant and the additive materials. The size of the additive material flakes (on the order of 1nm) are not representative of those that are expected to be present in the physical mixtures; however, do allow for more accessible and insightful calculation and evaluation. The modeled species are graphene sheets with functionalized groups added to be analogous the materials selected in this investigations; such as oxide, hydroxide, and carboxyl functionalized groups. Further discussion and comparison of the results observed by the molecular dynamics simulations by RxFF Consulting will not be made as these results were not ready for publication at the time of completion of this thesis. The information used in this thesis derived from work performed by RxFF Consulting has been used with explicit consent from the firm.

As expected across all additive materials, introducing more carbon material decreases the adiabatic flame temperature achievable by the propellant admixtures, as seen in Figure 3. The additive materials with oxygen containing functionalized sites experience a more gradual decrease in adiabatic flame temperature. This may suggest that the oxygen groups disassociate from the graphene sheets and oxidize some other reacting species; contributing to the energy release of the mixture.

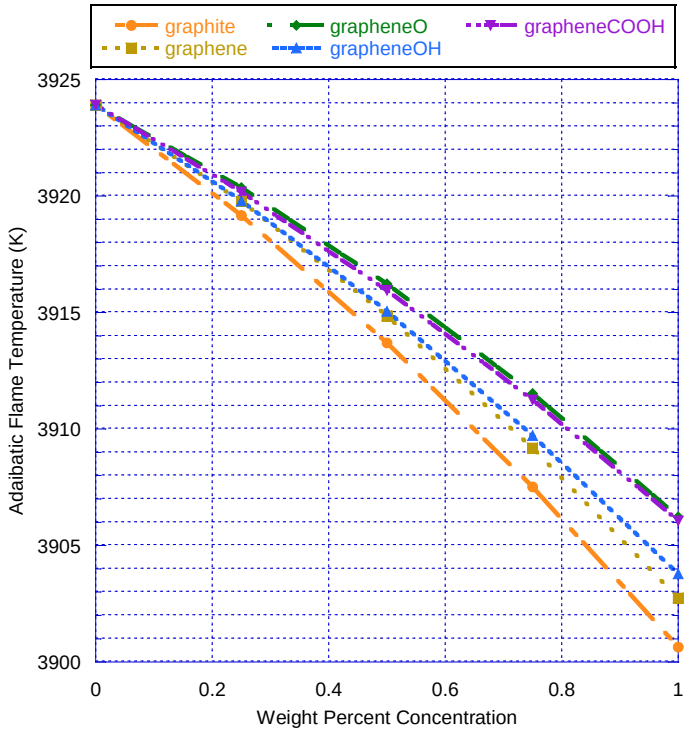

Figure 3: Calculated Adiabatic Flame Temperature

The steady decrease in the adiabatic flame temperature would suggest a decrease in the maximum work available from the propellant: a lower impetus. Figure 4 demonstrates that increasing the additive concentration very slightly increases the impetus of a propellant admixture. This slight increase is calculated to be at most 0.55% compared to the double base propellant with no additive. In a practical system, this increase would be negligible if not non-existent. One reason for the slight increase in propellant impetus is the addition of carbon into this system lowers the average mixture molecular weight, as carbon is less massive than the existing oxygen and nitrogen in the NC and NG molecules.

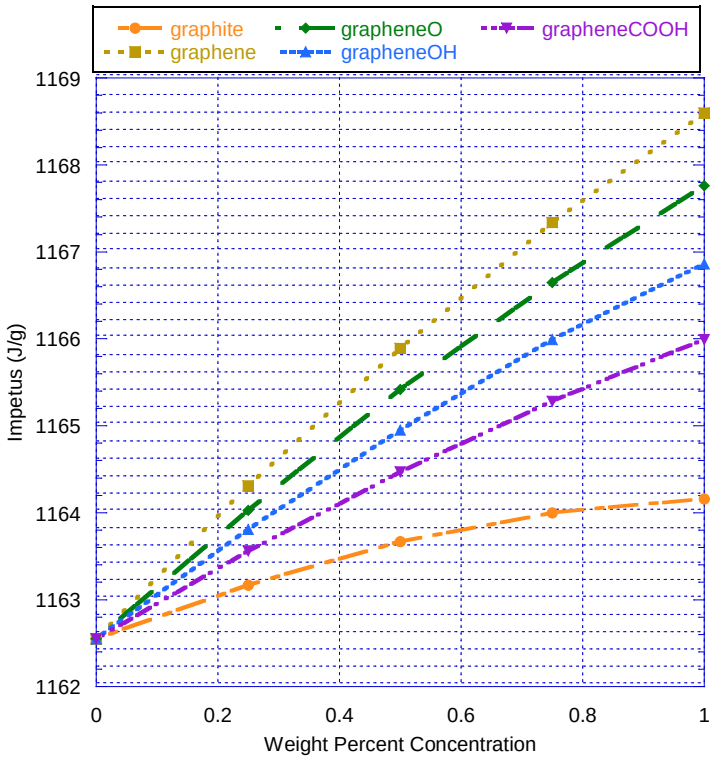

Figure 4: Calculated Propellant Impetus

Analyzing the results of Figure 4, reveal that increase in impetus is closely correlated to the relative abundance of hydrogen in the additive molecule. This makes sense, as the increase presence of hydrogen in the decomposed products would work to reduce the mixture molecular weight. In accordance to Equation 1, decreasing the mixture molecular weight leads to a larger value of propellant impetus. These hydrogen atoms are used to terminate the edges of the modeled graphene sheets, which is done to provide stable molecular dynamic simulations and calculations involving the graphene sheets. Real graphene particles do not need to be edge-terminated with hydrogen, which leads to purchased supplies of graphene materials to have considerably lower concentrations of hydrogen compared to these models. This observed increase may just be an artifact of the modelling.

RxFF Consulting has also performed simulations on the effects of graphene sheet size on NC and NG systems, and have modeled several sizes of non-functionalized graphene sheets. The

sheets are roughly similar in geometry (aspect ratio), and twice as large (sheet span) than the preceding size (~1, 3.5, 7 and 14 nm). The largest sheet size, 14nm, is still significantly smaller than any particle expected or seen of the purchased powders, as will be discussed in a subsequent section; however, these modeled sheets should give insights into the thermodynamic aspects of practical systems. With increasing sheet size, the relative abundance of hydrogen in the mixture will decrease and the behavior in adiabatic flame temperature and impetus should drift towards that of graphite. The trends in the effects of graphene sheet size and weight concentrations on the adiabatic flame temperature and propellant impetus are plotted in Figure 5 A and B, respectively.

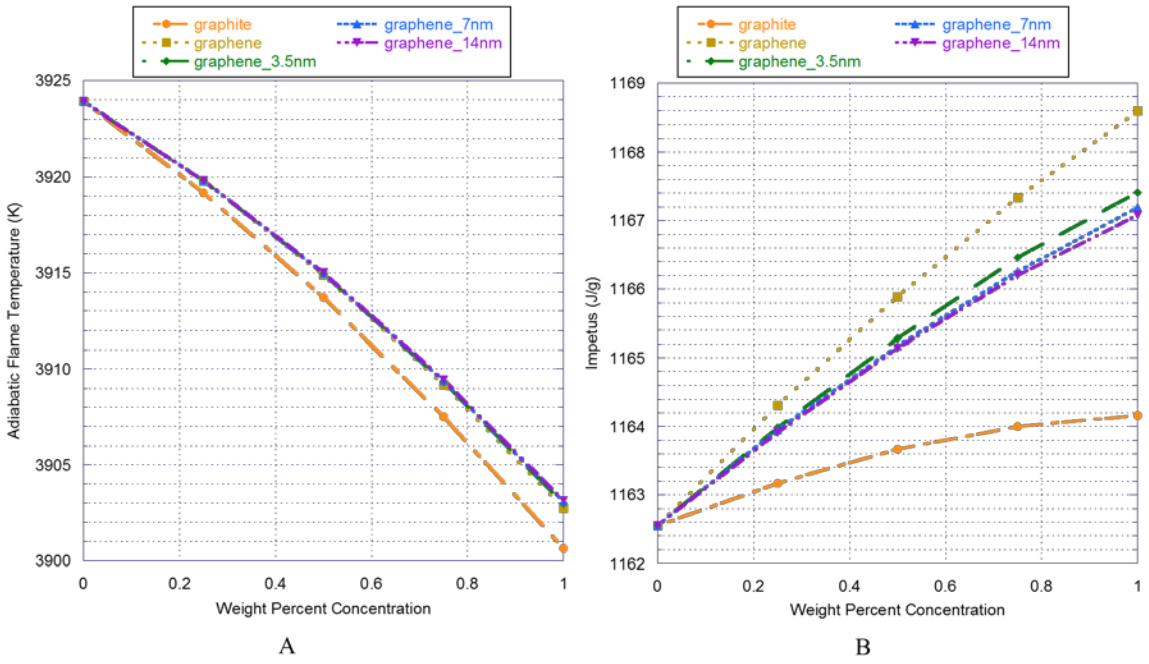

Figure 5: Effects of Graphene sheet size on A) Adiabatic Flame Temperature and B) Propellant Impetus

In Figure 5A, there is a clear distinction between how graphite and graphene effect trends in adiabatic flame temperature. All the graphene materials nearly collapse to a single curve. These two observations suggest that the offset seen in the adiabatic flame temperature with increasing concentration is due to the difference in heat of formation between graphite and graphene. This offset between the behavior in graphite and graphene is also seen in the propellant impetus

(Figure 5B); slightly higher adiabatic flame temperature leads to a corresponding increase in propellant impetus. Also seen in Figure 5B, the propellant impetus of graphene decreases with increasing sheet size. This behavior seems to validate the expectation that the decrease in the relative abundance of hydrogen allows the values of propellant impetus to drift towards that of graphite.

It is worth stating again that the size, morphology and exact composition of the modeled graphene additives are not expected to be fully representative of the purchased and utilized powders. These modeled flakes provide useful insight and expectation in behavior of these propellant mixes for the empirical testing and molecular simulations. Additionally, the calculations and simulations performed and discussed above are only a thermodynamic investigation to how the graphene additives would affect the energy output of the propellant. Catalytic behaviors that may be exhibited by these additive materials are not captured or considered.

The purpose of this discussion and supporting calculations is to demonstrate that energy output is not an appropriate metric of performance for the propellant mixture considered in this investigation. For the largest modeled graphene sheet, the increase in propellant impetus is less than 0.5%, which would be impractical to attempt to measure and obscured by other loss mechanisms already present in combustion systems. For this reason, the performance of propellant mixtures will be based off observed burning rates and characteristics of thermal decomposition. These measurements are experimentally obtained in controlled and repeatable setups. These procedures, described in later sections, will allow for direct comparisons of the effects of the graphite and graphene additives on the combustion of the DB admixtures.

Chapter 3

Sample Preparation

One of the greatest challenges of this investigation was the development of a propellant preparation process that would produce consistent and reliable test strands, which yielded representative data, and could be achieved within the scope and limitations of a lab setting. Much of the procedures described below were developed to be analogous to industrial processes at facilities such as BAE Systems at Radford Army Ammunition Plant (BAE/RFAAP). The much smaller batch sizes have presented several unique obstacles that are not typically encountered with large production facilities.

Overall, the developed process, from retrieval of the DB material from the magazine to analysis of test data, was optimized for a span of two weeks. Offsetting batch cycles by a week allows for weekly production and testing of propellants. This cadence has allowed for robust data sets and relatively quick turn around when implementing changes in the production procedure during the initial development. Each of the stages of the sample preparation are described in more detail in the subsequent sections.

Sonication and Mixing

The propellant preparation begins with the retrieval of the DB propellant strands stored in secured onsite propellant magazines. Each batch of tests varies from five to eight samples. The retrieved strands are individually weighed (±0.1g, Denver Instrument Company TL-12001), recorded, and assigned to specific test of a particular additive and concentration. With all the materials weighed and assigned, the appropriate amounts of each of the tested additives were weighed out (±0.001g, Denver Instrument Company TR-64) in individual 20mL scintillation

bottles. With the used scales and measurement uncertainty, the uncertainty in additive concentration is ±0.01wt%.

The scintillation bottles with the additive materials were filled with acetone to about two-thirds of full volume (~12 mL). The empty third is necessary during sonication, as the process can splash the acetone upwards along the walls of the bottle; therefore, this ullage ensures no acetone or additive material is displaced out of the bottle. A Branson Digital Sonifier S-450D was used for the particle disruption and breakup. Bottled samples were subjected to two rounds of sonication of 10s of an 80% duty cycle (0.8s ON, 0.2s OFF) at an amplitude of 35%. The use of the sonicator was intended to break up the additive particles to smaller sizes. The acoustic waves emitted by the probe is effective in making macro scale particles in acetone to a fine suspension.

Once sonicated, the additive mixtures were promptly transported to their respective containers with prepared DB propellant base material. The acetone and additive material were introduced to the pre-softened DB propellant and manually mixed. The large concentration of acetone promotes more rapid gelatinization of the DB propellant to a dough-like consistency, which allows for easier and more effective mixing. In the lab-scale process, the time between sonication and the various times the propellant is manually mixed was minimized to prevent any agglomeration of the sonicated particles.

In addition to the periodic manual mixing, the propellant mixtures were allowed to dry of the acetone solvent to firm up and plasticize. The quality of the final propellant product is very sensitive to the amount of acetone left within the propellant before the oven drying procedure, as will be discussed in succeeding sections. It is necessary to reduce the amount of solvent in the propellant mix as much as possible, and retain a degree of gelatinization to be formed and extruded. To achieve this, the propellant jars are left for periods of time with the lids off so that the acetone may diffuse to the open atmosphere. To speed up this process, the jars were occasionally placed in a simple oven held at 50°C. After approximately an hour with the lids

removed for drying, the jars are resealed and placed into the oven so that the acetone solvent within the propellant mixes reach equilibrium concentration. The mixes are again manually mixed and evaluated for firmness. This process was repeated until the propellant material is formable with a firm hand molding.

Propellant Plasticity

As will be discussed in subsequent sections, the quality of a tested strand (cylindricity and density) is heavily dependent on the amount of solvent present in propellant strands at the start of the drying section (immediately after extrusion). For reliable strand quality, the least amount of solvent is desired; however, some solvent must be present to maintain a level of gelatinization so that the propellant can be extruded. The optimized state of gelatinization was empirically determined to be to allow the propellant material to remain soft enough to manually form into a ball, yet dry and stiff enough that the ball maintains its shape without deforming under its own weight.

When the material has reached this state at a temperature of ~50°C, all jars of material for a batch to be extruded are kept in an oven of ~50°C until retrieved for extrusion. This step is done to ensure that the propellant admixes are isothermal and have a uniform concentration of solvent throughout. The warmer temperature allows the propellant to be softer and more easily extruded, leading to lower extrusion stresses[26], while utilizing less solvent. Uniform concentration promotes uniform drying and contraction of extruded strands leading to more reliable test data.

Extrusion

The use of a linear actuator (Parker 1894-1 ETS32-B05P-FM150-A) and stepper motor driver (Compumotor AX series) is necessary to achieve the quality and quantity of strands needed for thorough investigation. Previous manual systems were prototyped and experimented with; however, to use a less gelatinized consistency, the material is too stiff to reliably be pressed with human strength. Manual revisions were important in testing and verifying more specific design details like extruded diameter and plunger sealing. The fully automated extrusion system used for this investigation is depicted in Figure 6.

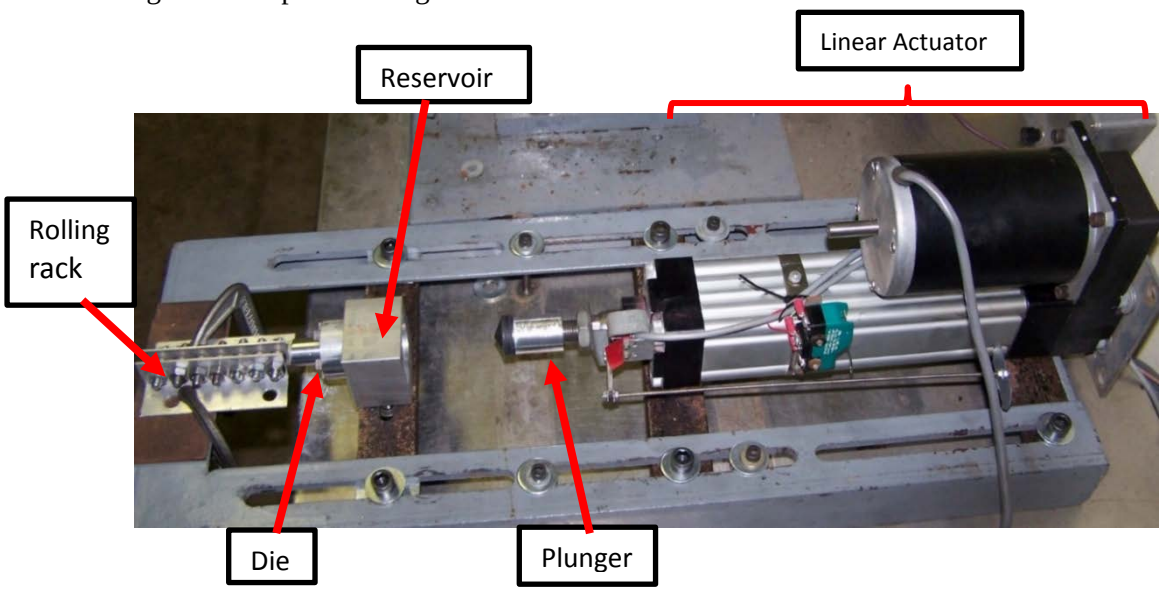

Figure 6: Automated Extruder System

The plunger is designed to mimic a plunger of a 60cc syringe used in prototyped manual extrusion systems. This was done to utilize the rubber plunger heads to ensure a good seal and compressible head against the propellant and die. The reservoir is not tightly fastened to the supporting angle iron. This is done for convenience, so the location of the reservoir relative to the extruder does not have to be reset every run, and allows for easier insertion of the plunger (ability to self-align).

The rolling rack is necessary to keep the extruded material as straight as possible after being extruded. The rollers consist of seven needle bearings to ensure the propellant strand are not inhibited from being extruded from die. It is clamped down for simplicity as this piece experiences minimal loads during nominal operations.

The die used in propellant extrusion, as depicted in Figure 6, was designed to produce uniform strands by optimizing parameters such as propellant gelatinization, linear actuator force, and resultant strand quality. Much of the information and guidance for the design of this component were derived from existing literature[26] and consultation with a research partner BAE/RFAAP. The mechanical design of the die is displayed in Appendix B. Die geometry (including total length and convergence angle) is crucial in controlling resultant product qualities such as extruded diameter, and surface finish. A desired aspect in the development of the propellant production process is to mimic existing commercial procedure in an attempt to replicate results and product quality of full-scale production.

More importantly, the diameter of the extruded strands must fit within the strand holder of the testing apparatus. The optical strand burner (as will be discussed in Chapter 5) has a propellant holder that accommodates strands of .25” diameter. The die diameter was empirically determined ~.23”, which allows for die swelling of the propellant material during extrusion, and material contraction during drying.

Safety

Extrusion of propellant materials presents several hazards during operation. Slightly elevated temperatures and pressures applied to an energetic material necessitates the consideration and implementation of several safety systems and protocols. The equipment and

procedures used presented many opportunities for mechanical, control and operational safety systems.

Physically, the entire extrusion system is located within a secure test cell. This test cell is constructed with 12” thick reinforced concrete wall, and shielded from the rest of the lab area by an outward opening blast door. The die of the extruder is pointed out a large bay door, which is opened to a fenced-off secured area during propellant extrusion. Additionally, the extruder is tightly fastened to a permanent workbench within the test cell. The secure location and fastening precautions are for reliability of the extrusion process and protection against damage to other lab equipment or injury to the operator.

The fastening of the die to the reservoir was also designed as a failsafe. The use of five 8-32 UNC aluminum bolts was selected for a designed factor of safety of two against the maximum actuator force. The over designing is to allow for secure fastening throughout repeated uses of the extruder yet not too excessive, so that the bolts will be the points of failure should the propellant ignite. As mentioned previously, the die during such an event would be ejected through the open bay door into an empty and secured area.

The motor controller and designed user interface program also contain limits to the travel of the linear actuator. Two mechanical switches were installed to the linear actuator to indicate the maximum forward and reverse travel limits of the actuator. The mechanical switches signal directly to the motor controller and will immediately stop actuator travel when either is pressed. The mechanical switches work in tandem with two redundant forms of software limits.

In the devised operation procedures for the extruding process, once communication has been established between the motor controller and control computer (located outside of the test cell), the absolute step count of the stepper motor is recorded at both limits of maximum travel. A serial command to the motor control ensures that the absolute step count of the motor will not

exceed the defined limits. The motor will immediately stop actuator travel if either limit is reached.

The other software actuation limit is imposed within the LabVIEW control program. The LabVIEW program serves as a more accessible user interface to the motor controller rather than direct serial communication. Unlike the mechanical and step limits imposed on the motor controller, the LabVIEW program does not directly affect the actuator, but restricts the commands sent by the operator. The control program ensures that a step command would not exceed the absolute step limit imposed. If a command is sent by the operator, an error message is displayed and no action taken by the actuator.

Increased Extrusion Lengths

As mentioned previously, the developed lab-scale process for preparing test samples has presented issues with producing materials that exhibit consistent properties (density and linear burning rate) from batch-to-batch and even strand-to-strand within a batch. The procedures laid out in this chapter work to promote and control the consistency and quality of the produced materials; however, the limitation in amount of material used in processing presents its own challenge. During the extrusion process, propellants experience a transient phase as the material is compacted by the linear actuator. This tends to lead to the initially extruded part of the strand to have poor cylindricity and surface roughness. Additionally, the ends of the strands experience a greater rate of solvent diffusion during the drying process (discussed in subsequent section), due to the larger exposed area, and exhibit a greater development of internal voids.

Commercial manufactures are able to get around these effects by producing large amounts of material. Longer lengths of extruded material allow for a greater proportion of the produced propellant strands that are not affected by the transient phase or ‘end effects’ regions.

Affected lengths of strands can be discarded. Utilizing grams of propellants, rather than tens of kilograms, in this lab-scale process means that a large portion of the produced strands are affected, and contribute to the inconsistency and scatter in collected data.

To investigate the effects of extrusion length on propellant properties, a batch of material was prepared with sample masses larger than previous batches to allow for a longer length of extruded propellant strands. The increase in prepared material was successful in producing strands that were nearly twice the usual length (~30cm rather than ~15cm). From visual observations, it was observed that the longer strands exhibited more uniformity in cylindricity and surface roughness. The expectation is that the extended extrusion strands would exhibit more consistent burning rates and thus less scatter in the data. To evaluate this, the standard deviation for Extended Batch, the current data set without Extended Batch data, and the complete data set were calculated for direct comparison. This comparison is shown in Table 3.

Table 3: Standard deviation Comparison

	Standard Deviation of Linear Burning Rate [mm/s]		
Material	Extended Batch	Data set w/o Extended Batch	Data set w/ Extended Batch
No Additive	2.3558	4.8840	3.9508
0.50wt% Graphite	3.1054	5.2258	4.3220
0.50wt% Graphene	1.0663	4.7612	4.2952
0.75wt% GOb	2.5793	6.6030	6.9016
0.25wt% COOH	2.1591	2.6363	2.4858
0.75wt% COOH	3.0640	2.4843	2.7240

For all but one admixture, 0.75wt% COOH, the standard deviation of the tests from the Extended Batch is less than the standard deviation of the current data set without the Extended Batch. This suggests that the strands from the Extended Batch do exhibit greater consistency in linear burning rate. The introduction of the Extended Batch data points with the rest of the data set reduces the total data set standard deviation; the exceptions are 0.75wt% COOH and 0.75wt%

GOb. Overall, it does appear that extruding larger volumes, resulting in longer strands of propellant, leads to greater consistency of linear burning rate results. This demonstrates that data scatter seen in this investigation is in some part inherent to the small amounts of material used in the lab-scale process. Increasing the amount of material extruded works to minimize but not eliminate the variability in propellant properties.

Drying

Upon extrusion, the propellant strands are immediately subjected to a managed and controlled drying process. This stage in the sample preparation is the most crucial in producing materials that are of high quality and yield usable and reliable data. Through trial and error, both accidental and controlled, it was recognized that the rate at which solvent diffuses from and through the propellant is the driving factor in the development of voids. Strands that were dried too quickly would suffer non-uniform contractions, which led to irregular surfaces and internal voids. The utilized drying procedure optimizes the quality of produced strands and the time necessary to achieve that quality.

Initially, the extruded strands are exposed to ambient conditions, which is the coolest temperature and slowest drying rate practically achievable in the lab-scale procedure. The propellant strands immediately after extrusion are still quite soft and most susceptible to void formation and surface irregularities due to non-uniform contractions. The strands are exposed to the ambient conditions for 24hrs, also during this time the propellant strands are periodically rotated to maintain cylindricity. After this time, the strands are placed within a small, ventilated oven to be subjected to a slow heating rate.

A temperature controller (Honeywell DC330E) with ramping capability allows for a controlled linear increase in oven temperature between desired set points over a specified

duration. To match the procedures done at large production facilities, such as BAE/RFAAP, a rate of 5°F/hr from 75°F to 140°F was applied to the propellants; however, strands suffered many internal voids and cavities, and many test strands yielded unusable data. This adverse effect is derived from the significant difference in drying chambers. Commercial facilities, such as BAE/RFAAP, have large buildings dedicated to heating large amounts of propellant; this room is also well ventilated. The dedicated oven being utilized (National Appliances Company, Mo. 5851) for drying these experimental samples is considerably smaller (45L) and essentially sealed (as the oven used is designed for vacuum purposes).

To adapt the procedure to better fit the systems being used, propellants are heated at 3°F/hr from 75°F to 145°F. The slower rate decreases the thermal/diffusion stresses within the strands and reduces the likelihood of forming occlusions. A slightly higher final temperature allows more solvent to be evaporated out and diffuse into the air in the oven. To deal with the volatilization of the solvent within the small confines of the oven, it was necessary that some form of forced ventilation be implemented in the small oven chamber.

Without ventilation, the volatilized solvent saturates the air within the oven chamber. The saturation stifles further diffusion of the solvent from the propellant; however, the temperature of the material continues to increase. The warm solvent is forced to expand and volatilized within the propellant material, leading the development of internal voids and occlusions. Having a continuous unsaturated (in regards to solvent vapor) source of air provides more uniform conditions within the oven chamber throughout the drying process.

For the lab scale processing at Penn State, ventilation was achieved by providing a low-level purge flow of air through the vent ports in the vacuum oven used for controlled elevated-temperature drying. The use of a commercial air compressor as a source allows a continuous low flow of “clean” air and does not require any tending throughout the multiple-day drying process. The commercial air compressor was later supplemented with a continuous flow fan, as the nearly

weeklong drying process is very taxing on the compressor motors. The flow rate is low enough that there is no effect on the maintained chamber temperature.

Following the drying procedure modification, subsequent batches of propellants dried in the oven exhibited improved quality. In addition, no volatilized substances condensed onto the inner surfaces of the oven. Previously, a small amount of nitroglycerin was found to have volatilized from the strands and deposited as a visible film on some of the cooler oven surfaces, such as the viewing window. The added airflow was sufficient to continuously clear out the gas-phase volatiles from the oven and maintain consistent conditions while drying.

The implementation of air ventilation in the oven during the drying process of the propellants has led to strands exhibiting significant reduction in voids and occlusions. This behavior has been consistent through multiple batches and additive materials. With less physical irregularities apparent and consistency in quality over time and samples, there is greater confidence that the data obtained of the burning rate of the materials dried with ventilation is more representative of the sample's actual behavior.

This confidence is further supported by observing the difference in measured burning rate data for batches processed with and without ventilation. Figure 7 depicts the observed burning rate of a few propellants for batches that were not dried with air ventilation (unfilled shapes) and batches that were dried with air ventilation (filled shapes). Additive and concentrations displayed in Figure 7 are those that have two or more burning rate data points for both batches not subjected to ventilation and batches subjected to ventilation.

One observation to make is that materials that were dried with ventilation experience less scattering in data points; this fact is plainly evident for 0.75 and 1.00wt% rGO. The dataset for these materials without ventilation show significant scatter which made it difficult, previously, to compare with other materials as the error bar range would be large. Batches that were dried with a ventilation exhibit more consistent burning behavior, though some scatter is still present.

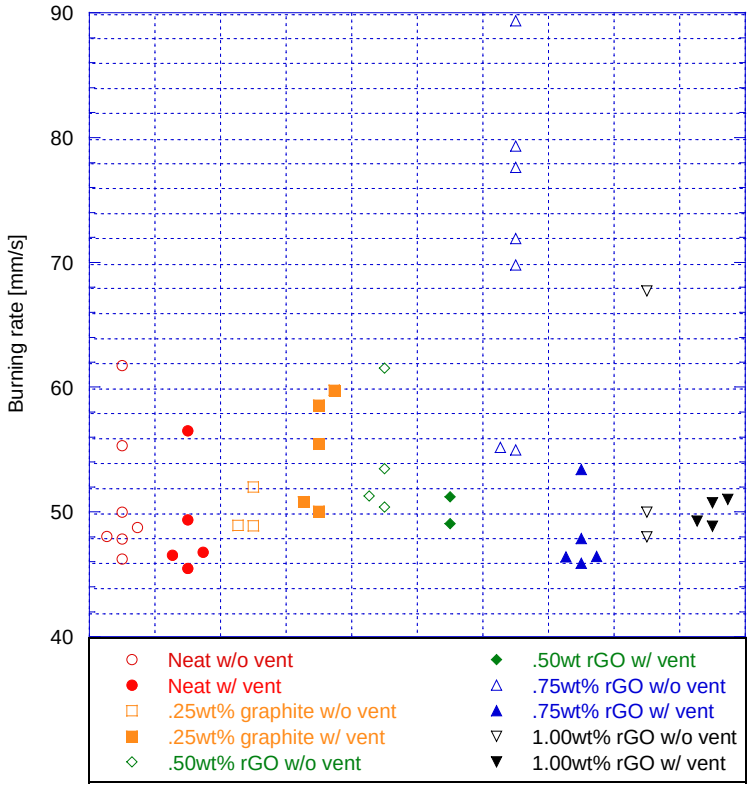

Figure 7: Comparison of burning behavior with and without ventilation

There appears to be some influence on the magnitude of burning rate on some samples. The DB with no additive, 0.50wt% and 1.00wt% rGO have groupings of data points with similar values of burning rate between batches that were and were not subjected to ventilation. However, 0.75wt% rGO and 0.25wt% graphite exhibit dramatic shifts in observed burning rate. 0.75wt% rGO has significantly lower burning rates after being dried with ventilation. This may suggest that without ventilation dried strands contained micro-voids which could have acted to increase the burning rate of the strand. Micro-void formation would not be uniform which would also support the very large scatter in the data for batches dried without ventilation. This logic does not hold when analyzing 0.25wt% graphene, which seems to increase in burning rate when dried under ventilation. This dataset is too small to make any sound speculation on the cause of this behavior.

Pre-test Preparation

Once the dried strands have been taken from the oven, they are prepped for strand burner testing. After extrusion and drying, the propellant strands measure in length between 14cm to 15.25cm (~5.5” to 6”). These are cut into three equal length segments each ranging from 4.4cm to 5cm (~1.75” to 2”), which allows for sufficient time and distance for video recording and analysis during burning regression. Cut segments (test strands) are kept in their respective order of the strand. This step is important in regards to tracking samples’ properties to the respective test data.

The cut and identified test strands are coated with a thin film of clear enamel. Solid propellant strands have a tendency for the burning surface to wrap around the cross-sectional area to the sides of the strand. This action effectively increases the burning surface area and can lead to faster, non-uniform burning of the propellant strand. To control this behavior, it is general practice to apply some form of inhibiting layer to the outer surface of the strand. A traditional[27] and easily available coating material is a clear acrylic: fingernail polish. This coating material proved to be ineffective as there was considerable issue with consistently applying thin layers. The acrylic layer had a tendency to not burn, creating a hallow tube as the propellant continued to regress. This had the effect of making the burning surface no longer visible to the camera, and greatly accelerated the burning rate of the propellant. The acrylic tubes seem to be sufficiently strong to withstand a higher pressure as the burning surface regressed, allowing them to act like a small pressure vessel. Both effects made data collecting unreliable or impossible.

Attempts were made to thin the acrylic to allow more uniform application of a thinner layer. This improved results but did not solve the problem. The solution used was applying a thin layer of spray, clear enamel (Rust-oleum Crystal Clear Enamel). The atomized spray allowed for uniform application of a very thin layer of coating. This inhibitor and application method has proven effective in terms of effort, cost, consistency and results.

Chapter 4

Material Characterization

Preliminary Thermal Stability/Chemical Compatibility Assessment

It is important to be sure that additives of interest are sufficiently stable when mixed with double-base propellant to ensure safety throughout sample processing and handling. Prior to propellant extrusion processes and mechanisms being implemented, a rudimentary assessment of the mixture thermal stability was performed.

This was done by gelatinizing four 1g samples of the DB propellant and adding 1wt% of the various graphene samples (GOa, rGO, Carboxyl FGS, one 'neat' DB sample used for control) sonicated and dispersed in approximately 12 mL acetone. These were hand-mixed until homogenous, and allowed to solidify and dry overnight. Each of the vials was encapsulated with a balloon and cinched shut, so that the balloon would act as a gas generation indicator (seen in Figure 8). Samples were aged in a 100 °C oven for one day (26hrs), which is similar to NATO STANAG 4147[28] Vacuum Thermal Stability test. This accelerated aging process simulates around a decade of aging. The samples after aging are shown in Figure 9.

Figure 8: Compatibility samples before placed in oven

Figure 9: Compatibility samples after aging in oven

There was no discernible difference between the volumes of the balloons from the start to the end of the assessment. This observation would indicate there was no gas generation or compatibility issues in any of the samples; however, this was not the case. Though the balloons did not melt in the oven at any point during the assessment, the material did become very sticky. This adhesion would be significant enough to inhibit inflation. This assessment was not particularly effective in qualifying if and how much gas was generated.

Upon closer inspection, bubbles were present in all of the aged samples (see Figure 10). As this assessment was performed prior to the establishment of the thorough drying procedure laid out in a previous section, most of these bubbles may have been from vaporizing solvent remaining in the propellant mixtures; however, the tested samples did not exhibit uniform internal void formation.

Figure 10: Closer examination of aged compatibility samples

The ‘neat’ DB propellant exhibited some bubbles during the accelerated aging process. Though not visible in the figure above, the sample containing carboxyl FGS exhibited a similar number of internal bubbles as the ‘neat’ DB propellant. This would indicate that the FGS additive is stable and exhibits little incompatibility at these relatively low temperature conditions.

As evident from the picture in Figure 10, the DB propellant with graphene oxide additive had considerably more bubbles throughout the sample. This suggests that the materials have some degree of incompatibility, which may indicate catalytic activity with the possibility of significant acceleration of the decomposition step in the combustion process. Without quantitative measurements, the magnitude of this instability is unknown.

The sample containing reduced graphene oxide additive in the DB propellant presents less obvious signs of reactivity. Instead of bubble formations, a ridge of material developed across the centerline of the sample. The rupture of a larger, singular bubble in the material may have caused this with the film making the ridge seen. If this is the reason for the ridge, this would suggest that, like the GO additive, rGO exhibits some degree of incompatibility or thermal instability greater than that of the control ‘neat’ DB propellant.

Based on this preliminary lab-scale assessment and an independent assessment by the propellant manufacturer, all additive materials examined were and are considered safe for use in lab-scale mixes. Since a reaction was observed under the accelerated aging protocol, there may be issues with long-term thermal stability of propellant formulations.

Thermogravimetric Analysis

Understanding the thermal stability and compatibility is important in characterizing the material for processing and storage; having a more precise means of observing the thermal decomposition of propellant mixes is of great importance in shedding insight on the fundamental behavior and interactions between the base propellant and the additive materials. To achieve this data, samples of propellant admixtures were subjected to thermogravimetric analysis (TGA). With the equipment, training and expertise available at Penn State Material Characterization Lab (MCL), precise measurements of the heat flux and mass loss as functions of temperature and time are obtainable using the TA Instruments SDT 2960 (displayed in Figure 11), which allows for simultaneous TGA and Differential Scanning Calorimetry (DSC) data collection.

Figure 11: TA Instruments SDT 2960

This machine obtains and calculates data by measuring the mass and temperature of crucibles on two different balance beams. These balance beams are thin, slender, extend several centimeters from their fulcrum, and are imbedded with a fine thermocouple (Pt-Pt Type R)[29]. The extension of the beams is to increase the sensitivity and precision (±0.1μm) in measuring the change in mass of the crucibles throughout the experiment. The imbedded thermocouples allows for precise (±0.5°C) and sensitive (ΔT= ±0.001°C) measurements of the temperature of each of the crucibles.

The heating profile selected for TGA experiments was chosen to closely match the profiles used in existing standards[28] (STANAG 4147 Test 3) and available literature[30] for direct comparison of obtained results, and to optimize the amount of time spent on the equipment. ~2mg of sample material was weighed out and placed into an open alumina crucibles with no lid applied. The alumina crucibles are thin walled and are very well characterized in terms of their thermal properties and behavior. For this reason, a clean alumina crucible is placed on one the

balance beams as a reference; any changes to mass and temperature experienced by the clean crucible can be removed from the changes in mass and temperature experienced by the crucible with the sample. A nitrogen purge flow of 100 mL/min is used to provide an inert atmosphere for heating and to clear generated gas from the test chamber.

Once the test has initiated, the sample is allowed to equilibrate to 25°C and held for 3 minutes. The sample is then heated to 100°C at a rate of 15°C/min. This relatively rapid heat rate is to limit the time spent on the machine. By observing results in available literature and some preliminary test runs, there was no observable changes in mass at 100°C, which allows for the rapid heating while minimizing the risk of any effect on material decomposition. The sample is then heated at a much slower rate at 2°C/min to 260°C. This much slower rate allows for greater investigation of the thermal decomposition of the sample, and is the prescribed heating rate used in standards and literature. To limit time spent on the machine, tests are terminated at this point though other literature results have tested DB propellants to upwards of 300°C. At the end of the test, the internal components of the machine are allowed to cool to 35°C before crucible cleaning and sample replacement for subsequent runs can be done. Overall, this process takes about one and a half hours to complete.

Before any data was collected for analysis, samples of the DB propellant with no additive were separately tested by the author and the thermal lab manager at Penn State MCL. This was done to qualify the author for independent operation of the TGA equipment, as well as verify the repeatability of the results from the testing procedure. The resulting curves were nearly exact and exhibited the same rates of decomposition and the same characteristic temperatures. This result validated that the TGA tests of these tests are reliably repeatable and fit for further analysis.

Sample Mass

During the initial training and evaluation of the DB propellant on the DSC-TGA instrument, samples of 35mg were used. The use of 35mg samples is a result of relying on a "default" configuration for the instrument. The typical amount of tested material for inert substances used is between 20 and 40mg, and as such, the first tests performed by the thermal lab manager and done as verification training with the lab manager utilized 35mg samples. Subsequent tests were therefore performed with 35mg for consistency. Concern arose during these experiments when seeing that all of the samples experienced very rapid decomposition (similar to that seen in Figure 12) and large heat flow.

It was identified that this behavior was the ignition propellant samples. When discussing the obtained results with other researchers with experience with double base propellants, they agreed that the ignition behavior seen indicates the 35mg sample size is too large for detailed thermal analysis of these energetic materials. Much smaller sample masses would allow the DSC-TGA instrument to better control temperature (avoiding thermal and reaction "runaway") and more accurately and precisely observe the thermal conditions.

After heeding this advice and investigating the minimum sample mass limitations of the instrument, it was determined that 2mg samples could be accurately tested. This value is the lower acceptable limit of the available DSC-TGA instrument at MCL, and is much closer to the presented guidelines of NATO STANAG 4147[28] Test 3 of 1mg. The same testing procedures as discussed above were used. Additionally, two samples of the baseline M9 with no additive were tested to validate obtained results. Both of those tests displayed nearly identical behavior which lent confidence to the ability for this procedure to capture the true behavior of the propellant. The resulting data obtained from this changes exhibited smooth and continuous decomposition, which (as will be discussed in later sections) is more characteristic of the true behavior of the DB

propellant. All of the samples tested and reported in this investigation are derived from 2mg samples.

Sample Geometry

During a verification test of the DB propellant with no additive, a drastically different behavior was observed. As seen in Figure 12, the solid red line indicates the first tested piece, which was cut as a thin piece off the remains of an extruded strand. This piece decomposed in a smooth and continuous manner. The dashed orange line is the behavior a piece of propellant cut to a small ‘chunk’ of material. This piece had a higher characteristic length, ratio of volume to surface area, than the initial thin piece. This characteristic seems to be significant in terms of the decomposition behavior, as this small ‘chunk’ underwent a rapid rate of decomposition and fully consumed the material.

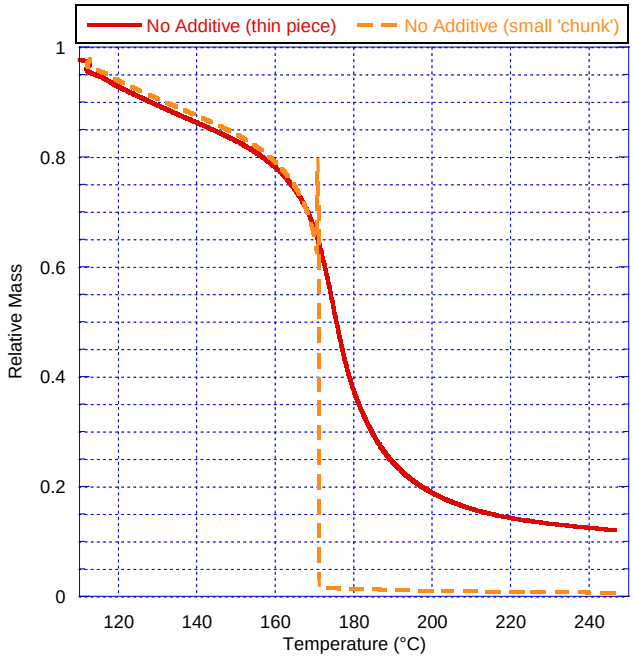

Figure 12: Effect of Sample Geometry on Decomposition Behavior

It makes intuitive sense that samples with a very low characteristic length exhibit a smoother, more gradual behavior, as the larger exposure to the chamber conditions and contact with the sample crucible ensure a uniform temperature throughout the material. It is also reasonable to think that material trapped within the interior of the piece could aid in the runaway ignition of a material; the propellant may decompose faster than those products, or generated heat, can diffuse to the surface. This issue is not experience by powders, as each particle has incredibly low values of characteristic lengths and decomposed products have a path to escape through the interstitial spaces between particles. Convection gives liquids a mechanism in which to effectively diffuse heat and species out and throughout the liquid.

All of the samples tested and reported in this investigation were prepared with this behavior in mind. Each sample was cut as a thin film-like piece from a remaining extruded strand. This will provide consistency in the results of all the tested propellant admixtures and should produce data that is more representative of the true decomposition behavior.

Additive Material Decomposition

Before analyzing the decomposition behavior of the propellant admixtures, it is insightful to observe the decomposition behavior of the stand-alone additive material powders. Understanding the thermal stability is important in evaluating the impact of these materials on the DB propellant and if there is risk in compromising the stability and safety of a propellant mixture, as some of the selected materials (GO, rGO, Carboxyl FGS) were specifically chosen for the potential interaction between the DB propellant and the functionalized groups. Each of the five selected carbon materials used in this investigation were subjected to the same TGA-DSC testing as laid out in a previous section. The measured relative mass loss from these tests are displayed in Figure 13.

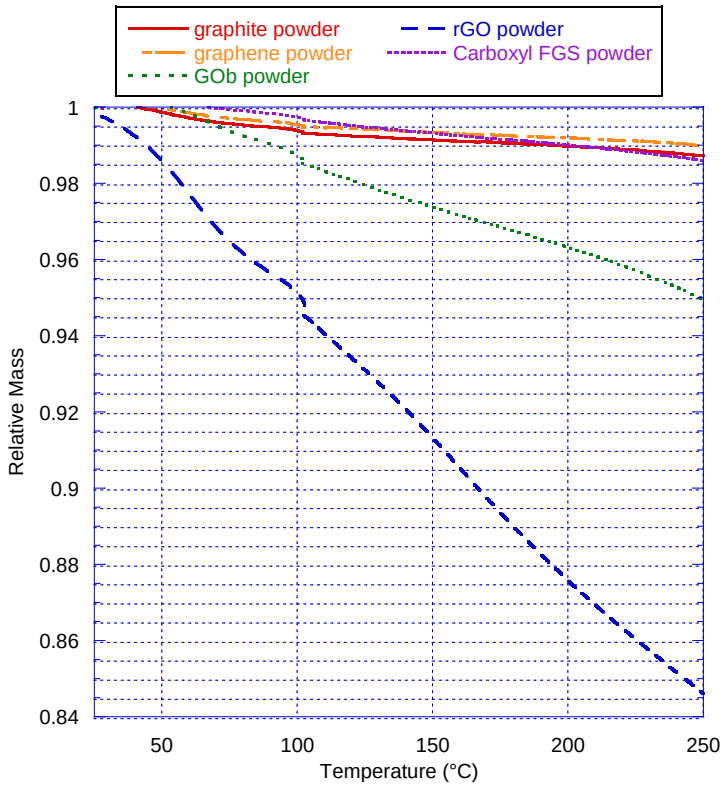

Figure 13: Thermal Decomposition of Additive Material Powders

There is a clear difference in thermal decomposition behavior between the additive materials, which appears related to the oxygen content of the carbon materials. Graphite, graphene and carboxyl FGS appear to be very stable and exhibit less than 2% mass decomposition over the entire tested temperature range. This thermal stability of graphite and graphene in an inert nitrogen environment is not too surprising, as these materials have been shown through various industries to be stable over a range of temperatures. The similar behavior exhibited by the carboxyl FGS seems to suggest it is also a stable carbon material even with the introduction of oxygen containing functional groups.

The GOb and rGO powders exhibit significantly greater decomposition across the tested temperature range. As mentioned previously from a review of graphene materials[15], oxide groups on graphene sheets have a tendency to decompose at relatively low temperatures. The decomposition curves in Figure 13 of GOb and rGO powders work to validate that statement. The

GOb powder exhibits a roughly 5% loss in mass while the rGO powder exhibits nearly three times that with roughly 15% loss in mass. This would suggest in a propellant mixture, as the mixture with GOb or rGO powders heat up, an influx of reactive oxygen species are introduced with the NC and NG components. This combination could allow for an early onset of ignition or increase the rate of decomposition of the propellant.

Strand Density Measurements

A simple and informative bulk material property is the density. What makes this property of interest in this investigation is the difficulty with strand quality and internal void formation as discussed in a previous section. Density can be utilized to standardize the linear burning rate data achieved during experimentation. Strands with more internal voids would exhibit a lower density as the same amount of material takes up a slightly larger volume. These strands are also likely to burn faster as the flame front encounter the internal voids and thus greater surface area exposed to the flame. The inverse relations would be true for strands that contain no internal voids. By multiplying the strand density to the measured burning rate of that strand, the resulted mass burning rate of the burning propellant would be more representative of the true nature of the material.

To calculate the density of each test sample, the mass and volume must be measured. Mass is easily measured and recorded by utilizing the readily available precision laboratory balance (Denver Instrument Company TR-64) to a precision of ±.0001g. Conversely, accurately and quickly measuring the volume of each test strand posed more of an issue. High-precision laser/optical scanning instruments are available at Penn State MCL; however, obtaining these measurements for each test strand in a batch (~20) would be prohibitive in terms of cost and time.

A very simple and easy method of measuring density is by means of water displacement. The volume measurement occurs after the samples have been cut to length and coated with the enamel inhibitor, which functions as a water-sealing coat. Strands are only submerged for the time necessary to make the measurement, then quickly dried of any external water and allowed to air-dry at ambient temperature. However, a great disadvantage to this system is the resulting uncertainty of the measurement when made without specialized hardware. Using a standard 10mL graduated cylinder (for a sample of approximately 1.2cm^3), the uncertainty of a volume measurement is ±0.1mL, which is roughly 10% error in volume. With the uncertainty measurements for mass and burning rate, the calculated mass burning rate could have an uncertainty of up to ~12%, most of which driven by the uncertainty of volume. To greatly reduce this uncertainty in the volume measurements, a specific gravity bottle (Humboldt H-2640 24mL Hubbard specific gravity bottle) was purchased and used. An image of a 25mL Hubbard style specific gravity bottle much like the one purchased can be seen in Figure 14.

Figure 14: 25mL Hubbard specific gravity bottle

The bottle is designed to hold 24mL and meet ASTM D1429. This standard also provided great reference for proper filling, usage and measuring of the bottle. However, the least discussed aspect of the bottle use is the removal of excess fluid from the bottle once the cap has been put on. The bottle is filled using a simple syringe for the 25mL volume, but bit of excess fluid is warranted to utilize the precision design of the capillary tube in the cap. The excess fluid ensures

that the bottle will be completely full; however this excess fluid must be cleaned off and the bottle dried for weighing.

Much of the available literature glosses over this matter and simple states to ‘wipe the bottle dry before weighing’. When following these instructions, the measured mass of the bottle filled with water was inconsistent with measurements with a range of 0.075g. It was found that by using a paper towel to dry the cap of the bottle, water within the capillary tube would be pulled out and compromise the precise volume of the bottle. To overcome this, a flat blade was used to push and wipe any excess water from the cap. Using this method and the measuring method laid out in ASTM D1429, the masses can be reported with an accuracy of ±.02g (± .03%).

In addition to the precision weigh scale and specific gravity bottle, the temperature of the water used was monitored and controlled within a circulating bath. A K-type thermocouple was used to record the temperature of the bath with a precision of ±0.1°C after each material was tested. A large beaker of distilled water is submerged in the circulating bath to be used specifically for filling the specific gravity bottle. Throughout the usage of the water during weighing, the temperature did vary, but no more than the allowed deviation of ASTM D1429 (8.1). This control and precision is necessary in obtaining the correct value of the density of liquid water. These values were obtained using the saturated water tables at 1atm available through NIST WebBook.

The volume of displaced water was calculated by subtracting the mass of the bottle filled with water and a sample strand from the mass of the bottle filled with water and the stand-alone mass of the strand, all of which is divided by the density of water at the room temperature (measured after each weighing). This can be seen in the following Equation 2, in which the subscripts BW represent mass of the specific gravity bottle filled with just water, S is the stand-alone mass of the strand, and BWS is the mass of the bottle filled with water and a strand.

Equation 3 is used to solve for the density of each test strand using the calculated volume of displaced water and the measured mass of the strand.

$$V_w = \frac{m_{BW} + m_S - m_{BWS}}{\rho_W} \quad (2)$$

$$\rho_S = \frac{m_S}{V_w} \quad (3)$$

With the other measurement uncertainties of the weigh scale and temperature, the percent uncertainty of the strand densities is approximately .04%, which is nearly four orders of magnitude smaller than the previous method used (~12%).

Powder Density

One of the useful insights that density measurements of each strand can provide is the potential presence of internal voids. As mentioned in the previous chapter, the drying process is specifically tailored to minimize the formation of micro-voids and occlusions from forming within the strands. One indication of how successful those efforts are is observing the frequency of usable strands and the scatter of burning rate data; however, this is more of a qualitative comparison on the performance of dried strands. To get a quantitative idea on the potential presence of micro-voids within strands, the theoretical densities of each propellant admixtures for each additive material and concentration must be calculated and compared to the measured densities of each propellant admixtures.

One of the more challenging aspects of calculating the theoretical densities for the admixtures is obtaining a powder density for the additive materials, particularly measuring the volume occupied by additive materials. This was achieved using the specific gravity bottle in a very similar manner as described above. A small amount of additive (~.035g, similar to amounts used in 0.25wt% concentrations) was weighed out into a scintillation bottle, and recorded. The

scintillation bottle is filled with roughly two thirds of ethanol so the additive can be sonicated in the same manner as laid out in the Sample Preparations chapter. Ethanol was selected as a solvent for a number of reasons; firstly, it is a standard solvent used for the measurement of powder density, as it behaves as a non-polar substance, unlike water, which would prevent bubbles from being captured within the powder. Additionally, ethanol is less volatile than other solvents used, such as acetone, which allows for more reliable and accurate measuring the mass of a filled specific gravity bottle.

The particles are sonicated so that the measured volume displacement is most like that of how the powder is used in mixing. The process also works to drive out any remaining bubbles within small piles of powder in the bottle, and separates particles so each can be fully wetted. Once sonicated, the slurry is transferred to the specific gravity bottle, and given an opportunity to settle. This settling is done in an attempt to clear the upper region of ethanol of particles. As explained in the previous section, the bottle is overfilled slightly so that excess liquid can be wiped away and ensure 25mL is contained in the bottle. Knowing that some amount of ethanol in the bottle would be lost, the settling effort was done to minimize the loss of additive material within that lost liquid, and ensure that the measured amount of material remains in the bottle. With the procedure and consideration made above the measured powder densities and measurement uncertainty are displayed in Table 4.

Table 4: Measured powder density

Material	**Density (g/cm^3)**	**Measurement uncertainty (± g/cm^3)**
Graphite	1.063	$3.11*10^{-3}$
Graphene	0.812	$3.09*10^{-3}$
GOb	0.359	$3.11*10^{-3}$
rGO	0.315	$3.27*10^{-3}$
Carboxyl FGS	0.325	$2.52*10^{-3}$

The relatively small densities values obtained in the measurements prompted re-measuring of all the additives. However, subsequent measurements of each material fell within the measurement error from the initial measurement. This fact lends validity to the initial measurements and confidence that the value captures the true nature of the particles. With these measurements, the theoretical density for each material and concentration can be calculated using Equation 4, where Y is the component mass fraction and ρ is the component mass density. The results of the calculations are displayed in Table 5.

$$\rho_{mix} = \left(\frac{Y_{add}}{\rho_{add}} + \frac{Y_{DB}}{\rho_{DB}}\right)^{-1} \quad (4)$$

Table 5: Theoretical Density of Propellant Admixtures

	Density (g/cm^3)			
	Concentration			
Material	0.25wt%	0.50wt%	0.75wt%	1.00wt%
Graphite	1.631	1.629	1.626	1.624
Graphene	1.629	1.625	1.621	1.617
GOb	1.619	1.604	1.591	1.577
rGO	1.616	1.599	1.583	1.567
Carboxyl FGS	1.617	1.601	1.585	1.570
DB with No Additive		1.633 (±0.000)		

Comparing the theoretical values calculated in Table 5 to the experimentally obtained measurements from produced strands will give insight on the relative prevalence of micro-voids and occlusions within strands, and what affect different additives may have on that behavior. Additionally, the comparison will serve as a check on the effectiveness of the lab-scale production process in creating propellant strands as close to propellant properties obtained by commercial manufacturers, such as BAE/RFAAP. The density value of the DB propellant with no additive is from the stock material retrieved from on-site magazines, produced by BAE/RFAAP.

Scanning Electron Microscope Imagery

Physical imaging of the microstructure of the propellant admixes and standalone particles gives valuable insight on the structure of the propellant after extrusion, particle size, and distribution of additive material. To obtain these images, a scanning electron microscope (SEM) available at Penn State MCL was utilized. The high magnification and resolution images allow for analysis of additive particle sizing and distribution within the DB matrix. Having qualitative and quantitative evaluation of particle distribution in the propellant matrix can assist with assessing material processing, matching or refining models, or identify the need to increase sonication of additives during sample preparation.

To get “undisturbed” sample surfaces suitable for appropriately assessing the mixes of polymeric materials (similar in behavior to the cellulosic double-base propellant matrix), it is generally desirable to generate a clean fracture. The plastic nature of the DB material ruled out cutting with a knife or microtome, since the matrix structure and embedded particle features of interest would be torn or “smeared”. Therefore, cryogenic fracturing was used.

To cryogenically fracture the samples, they were first submerged in liquid nitrogen in a small open mouth Dewar flask and allowed to completely chill to the liquid temperature. The temperature of the sample was chilled well below the brittle transition temperature and the sample could then be easily broken under application of a small amount of mechanical bending or compression force. For the best imaging practices, the samples need flat and cleanly broken surfaces for observation.

In addition to images of propellant admixtures, images were taken of sonicated particles on silicon wafers. As mentioned previously, this was done to qualify and quantify the particle size after being subjected to sonication. The powder materials were subjected to the exact same sonication process as laid out in a previous section, then a drop of the acetone-additive slurry was

dripped onto silicon wafers, which have surface roughness much smaller than the sizes of any particles in this investigation. The acetone is allowed to evaporate from the wafers leaving only the particles behind for viewing. The vaporization process did prove to have some adverse effects. As the solvent evaporated, the surface tension of the remaining liquid tended to drag and conglomerate particles as the liquid drop rescinded. For some of the images, this gives a biased impression of poor distribution, as will be discussed below.

“Neat” reprocessed DB propellant

Reprocessed DB propellant with no additive can be seen in Figure 15. These images are being used to identify the structure and features of the double-base matrix, and for comparison with images that contain additives. As can be seen in the image, the propellant is amorphous with a fiber quality; this is consistent with many polymer materials. However, these images reveal that the propellant produced in the extrusion procedure contains micro-voids and clumps. The obtained images were sent to the propellant manufacture for consulting and reference. It was stated that some of the surface features observed are indicative of fractured nitrocellulose surfaces, particularly considering the surface pitting features and the relatively amorphous, wavy, surface pattern. As the image comparison was based off similar but different propellant compositions, only qualitative comparison can be made to validate and verify that the material observed in this investigation is representative of the true nature of the DB propellant.

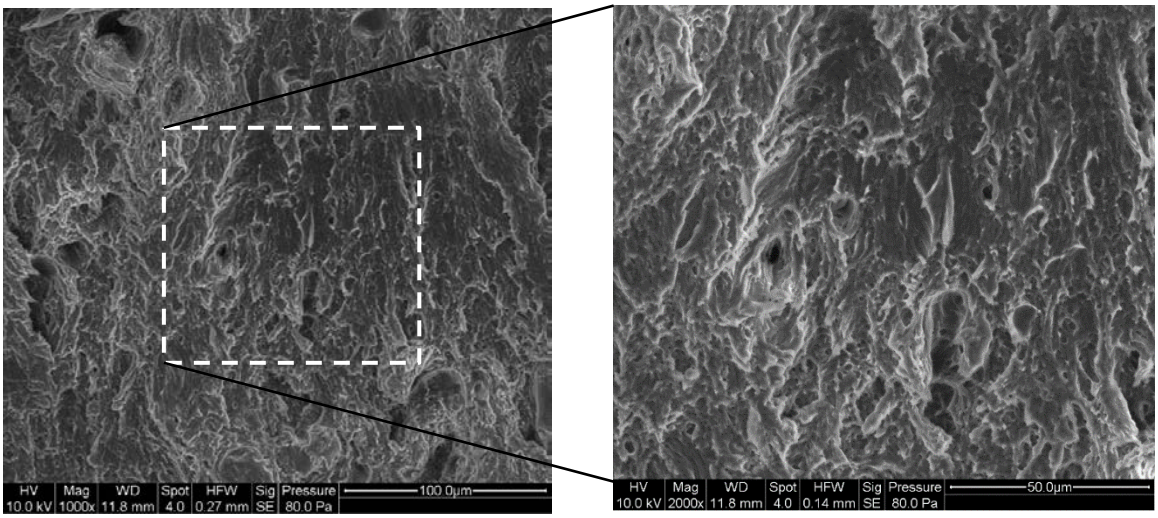

Figure 15: SEM Images of DB with no additive

Another important aspect of Figure 15 is to visually characterize the DB matrix in the SEM images. Though the additive powders and the DB propellant have optically different parameters such as color and transparency, these differences may be eliminated when the materials are homogenously mixed and observed at non-optical wavelengths. From the direct scanning electron beam, the DB matrix appears as a matte gray surface with darker areas indicating deeper crevices and lighter areas indicating higher ridges. In the back scattering images (to be seen in subsequent figures), the DB matrix appears as a static, black background. These basic observations will allow for detection and evaluation of mixed particles.

Graphite

The graphite particles experienced some of the conglomeration due to the solvent surface tension as mentioned above. This behavior as well as any natural agglomeration experienced by the particles in the scintillation bottles after sonication leads to relatively large collections of small particles, as can be seen in Figure 16. Also visible in this image are very small (~1µm)

isolated particles across the wafer and slightly larger (~10μm) groupings. This image is reassuring that graphite product supplied by Asbury can be treated to produce very fine particles.

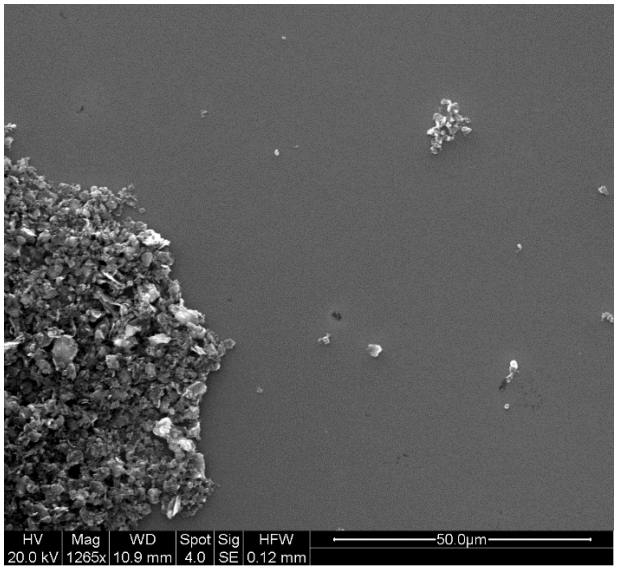

Figure 16: SEM Image of graphite particles

Graphite particles within the DB matrix provided some challenge in differentiating between the two in the standard SEM view. Both of the image sets presented below utilize Back Scattering Electron (BSE) images. In this setting, the carbon additives (white) are very distinct from the DB matrix (gray).

Figure 17 depicts a cross section of a piece of 0.75wt% graphite sample. In the lower magnification image on the left, it is apparent that the graphite has some denser groupings of material located sporadically through the matrix. This may suggest that after sonication and during gelatinization of the mixture, some of the particles started to agglomerate into more dense groups rather than being homogeneously disbursed and mixed.

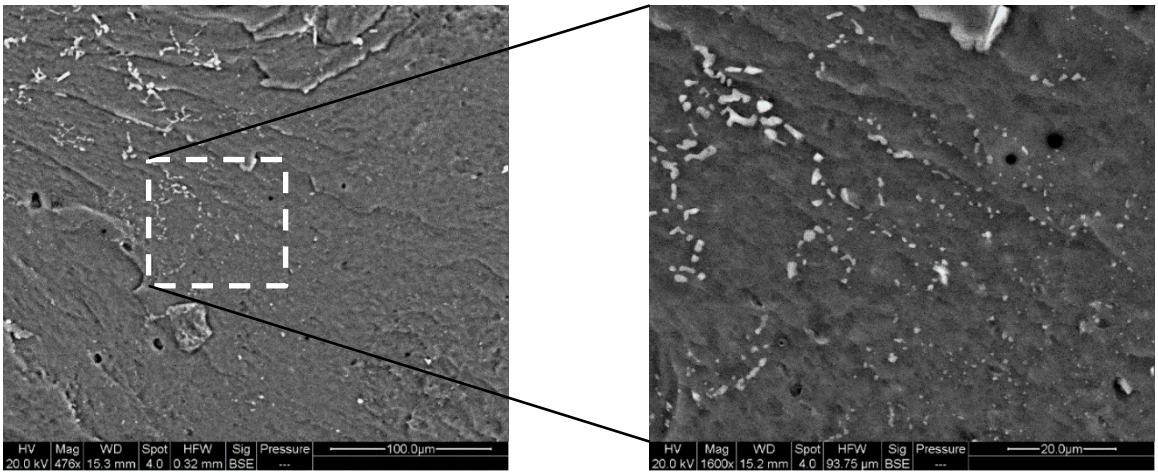

Figure 17: BSE imagery of 0.75wt% graphite

The higher magnification image on the right shows how fine some of the particles are. Each of the tiny white specs in the image is a graphite particle; this image depicts particles clearly less than 1µm in size. These tiny particles and their roughly homogeneous distribution were seen in other observed location on the sample piece. The large conglomeration of particles seen in Figure 16 are not apparent in Figure 17 lending assurance that the agglomeration is due to the surface tension of the solvent.

It is important to note that the particles seen in Figure 16 and Figure 17 are considerably smaller than the producer specified particle size. The military specifications[15] for this graphite material, Grade 4, is only defined that at least 96% of the particles pass through US standard sieve No. 225, with pore sizes of 44µm. This may suggest that other supplies or batches of this graphite material may contain higher concentrations of the larger size particles, and that the effect on the combustion behavior of the propellant admixtures may differ from those obtained in this investigation.

Graphene

The prepared graphene particles did not seem to conglomerate on the wafer in the same way as the graphite particle sample, potentially due to the flake-like morphology. The graphene particles in Figure 18 appear to be approximately 30μm in size, with some ~10μm particles visible but no apparent sign of smaller particles. The visible particles do not appear to be solitary particles of graphene but clumps of smaller graphene flakes. The small clumps of flakes could be a results of solvent vaporization or could indicate a more rigorous dispersion process (long duration or higher amplitude sonication) may achieve finer particles.

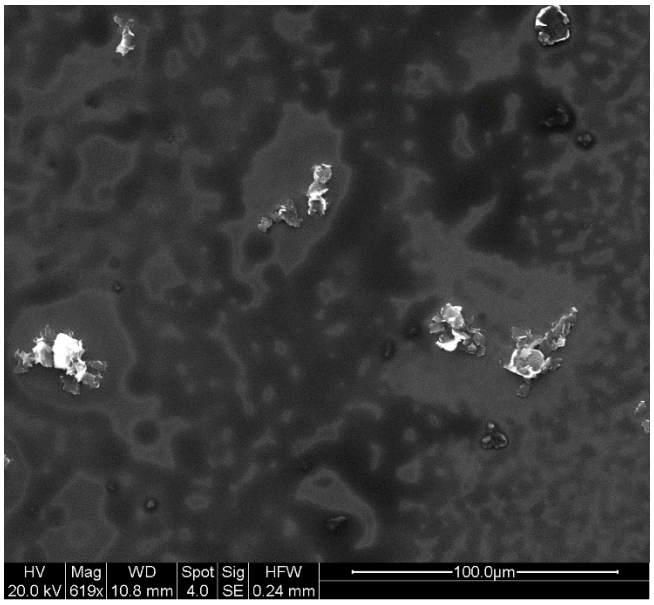

Figure 18: SEM Image of graphene particles

Figure 19 shows a magnified view of a fractured surface of the DB propellant with 1.00wt% graphene additive. Similar to the images of the graphite propellant admixture, the graphene additive blends fairly well with the DB matrix, and only appear slightly brighter. The first image (200x) shows decent dispersion of the relatively large (~100μm) flake-like particles within the matrix. From this low-magnification image, there is no apparent agglomeration of

particles suggesting good breakup and dispersion in the solvent before addition. On inspection of the higher-magnification (1000x) image, the visible particles appear to be solitary flakes and not agglomerates of finer flakes as seen in Figure 18. This may be due to physical stress from mixing in the propellant to break apart particle agglomerations as intended.

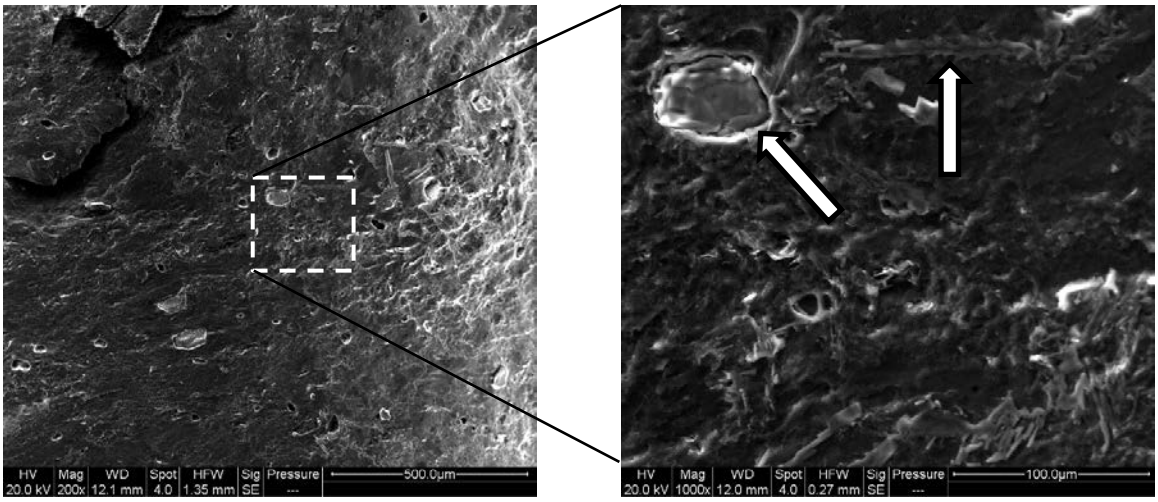

Figure 19: SEM Images of 1.00wt% Graphene

The density of particles in the DB matrix may be higher as some particles are embedded edge-on (pointed out by right most arrow in Figure 19). These edge-on particles are much less apparent at lower magnification due to the very thin nature of the graphene platelets. Figure 18 and Figure 19 are in contrast with one another on the size of particles achieved from particle sonication and processing. Figure 18 does not show particles as large as the multiple flakes visible in lower magnification image of Figure 19. It is unknown why these larger particles are present and relatively abundant. The higher magnification image of Figure 19 does not show many particles similar in size to those seen in Figure 18; however, this may be due to the subtle difference in shades between the particles and DB matrix.

Graphene oxide

Compared to the rest of the obtained and purchased additives, GOa was composed of small flakes visible to the naked eye, rather than fine powders with distinct particles only discernable under microscopic inspection. As such, this material was treated to longer exposures of probe sonication (30s rather than the typical 20s on the other additives) in an attempt to disperse the flakes into smaller particles. Nevertheless, it was expected that this material, even with the additional treatment, would have the largest particles and sparsest distribution. Figure 20 supports some of these expectations. Not as many particles are apparent in the zoomed out image of Figure 20 compared to that of graphene in Figure 19. Additionally, the single particle visible in the zoomed in image of Figure 20 is considerably larger than the graphene particles of Figure 19.

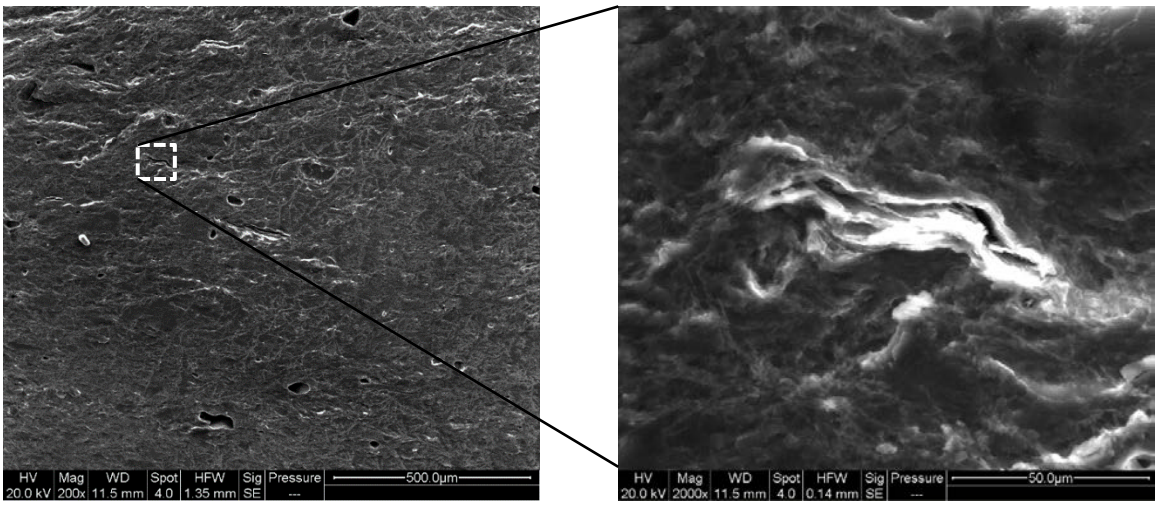

Figure 20: SEM Images 1.00wt% GOa

An interesting observation of this image is the internal delamination of the GOa flake. It can be seen in Figure 20 that the GO flake has been separated and some of the layers are distributed across the thickness. This structure, believed to result from the manufacturing process, may be detrimental to propellant stability by providing a void or pocket within the propellant that could be susceptible to shock initiation or decomposition product accumulation.

As mentioned previously, the undesirable flake size, adverse compatibility indication, and great difficulty in obtaining burning rate data, an order for additional material was purchased from a different supplier, Garmor. This powder is advertised as having an average particle diameter of 500nm and is a very fine powder. The new supply of GO (GOb) was subjected to the same evaluation the other additive materials were subjected to. SEM images of the GOb material are displayed in Figure 21.

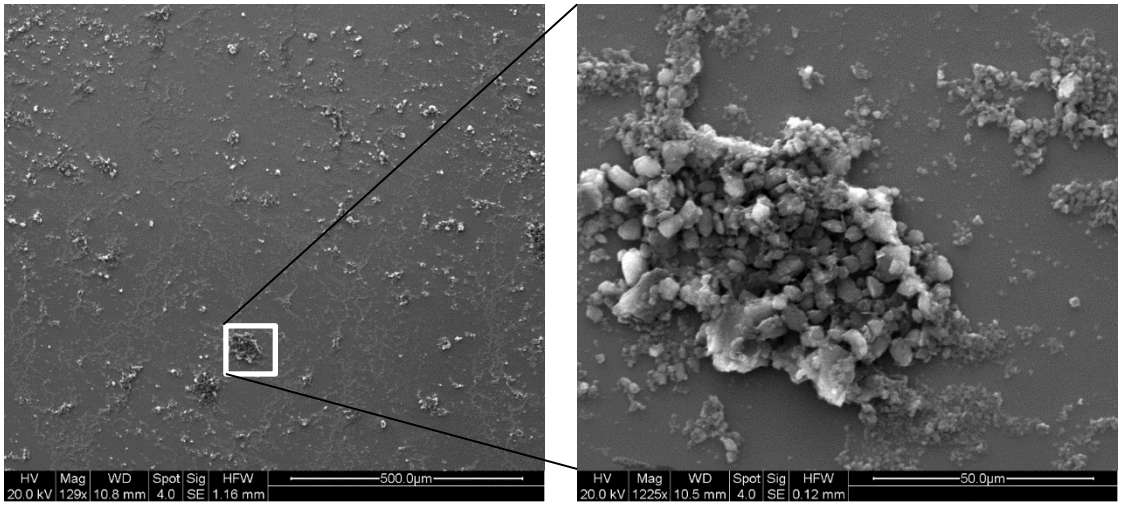

Figure 21: SEM Images of GOb particles

The range of particle sizes visible in Figure 21 is quite varied. There is a conglomerate on the order of 50µm in length and an assortment of solitary particles on the order of 1µm or less. The conglomerate seen in this image is a result of the surface tension of the evaporating solvent dragging particles together. This can be said with certainty, as there were many ‘rivers’ and ‘trails ’of particles visible in the lower magnification images. These features give a clear picture of the particle behavior and conglomeration during the evaporation of the solvent.

Images of 0.50wt% GOb in Figure 22 also reveal small particle sizes and even distribution of the GOb additive in the DB propellant. In the lower magnification image on the left, individual particles are less apparent. In this instance, this is favorable as there are no large particles or denser groupings of smaller particles. This also lends validity that the

conglomerations seen in Figure 21 are an artifact of the silicon wafer presentation and not wholly representative of particles subjected to mixing procedures. The higher magnification image on the right upholds that initial impression. At 872x magnification, small, evenly distributed particles cover the matrix. In the right image of Figure 22 particles no larger than 10μm can be seen; however, in other parts of the sample pieces there were pieces approximately 40μm across.

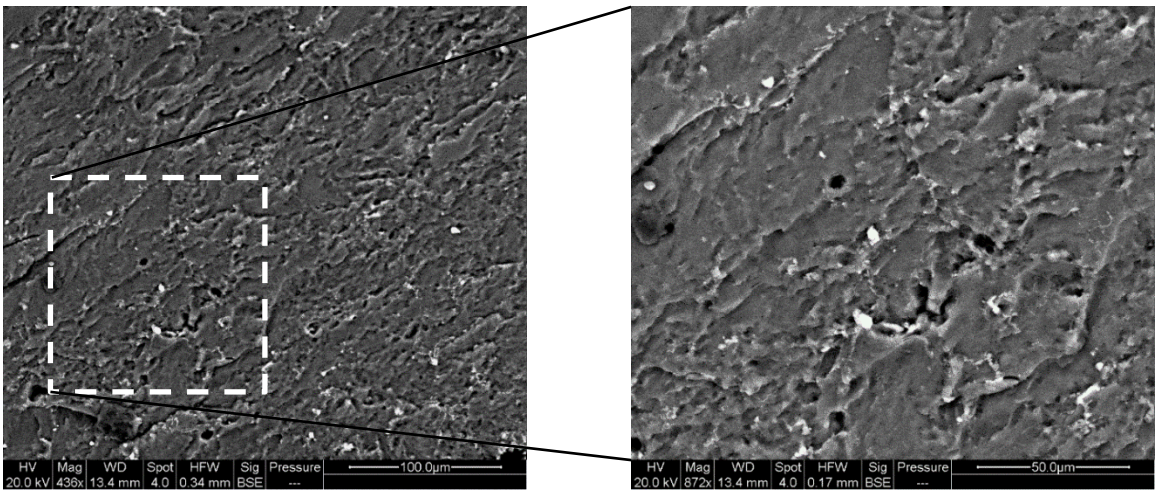

Figure 22: BSE Images of 0.50wt% GOb

The particle size and distribution for this sample and the particle images in Figure 22 are superior to that of the previous supply of graphene oxide (GOa). These images validate the change of provider and give some insight to the inconsistency in burning rate data (or lack thereof) and very poor strand quality exhibited by GOa samples. All further material and burning rate analysis analyzed in this thesis will utilize GOb as the representative admixture on the effects of graphene oxide on the behavior and properties of the DB propellant.

Reduced Graphene Oxide

The supply of rGO powder purchased from Cheap Tubes Inc. demonstrate very clear signs of consisting of very fine particles. When retrieved for material processing, the powder is susceptible to influences of minor air currents before dispersion or mixing. This attribute made

handling the powder a little more of a chore, but suggested great potential for fine particles and dispersion within the DB propellant. The SEM images taken of the isolated rGO particles (seen in Figure 23) do validate that potential.

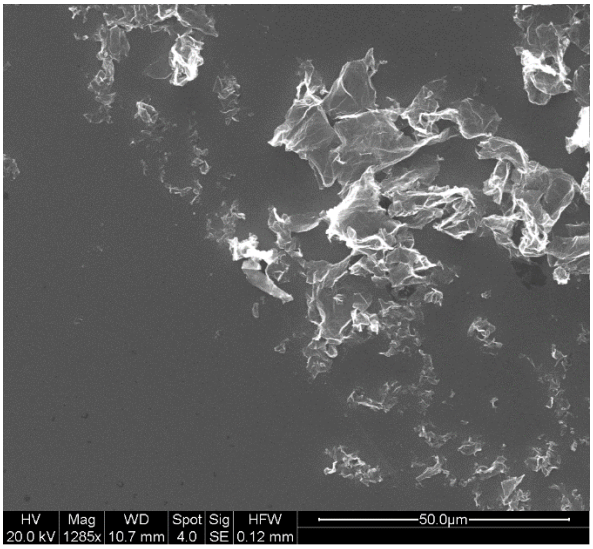

Figure 23: SEM Image of rGO particles

What is remarkable about the material seen in Figure 23 is that the rGO particles are more akin to single large sheets. Sheets would provide for much higher contact surface area with the DB propellant and may facilitate a more pronounced influence on combustion behavior. The range in particle size visible in Figure 23 seem to demonstrate the sonication process works to break up some of these sheets (~50µm) to even smaller pieces (~1µm). To understand if these exhibited properties of the isolated particles is representative of the additive within the DB matrix; images of the admixture are needed.

Figure 24 shows magnified images of DB propellant with 0.50wt% rGO. In contrast to Figure 23, there appear to be much larger flakes (~100µm compared to ~50µm) of rGO within the DB matrix. This difference may be due to some agglomeration during the mixing process. The higher surface area sheets seen in Figure 23 would have a greater tendency to adhere to other sheets, which could lead to larger particles within the propellant admixture. The higher

magnification image in Figure 24 does reveal that very fine particles (~5μm) of rGO are present and well dispersed.

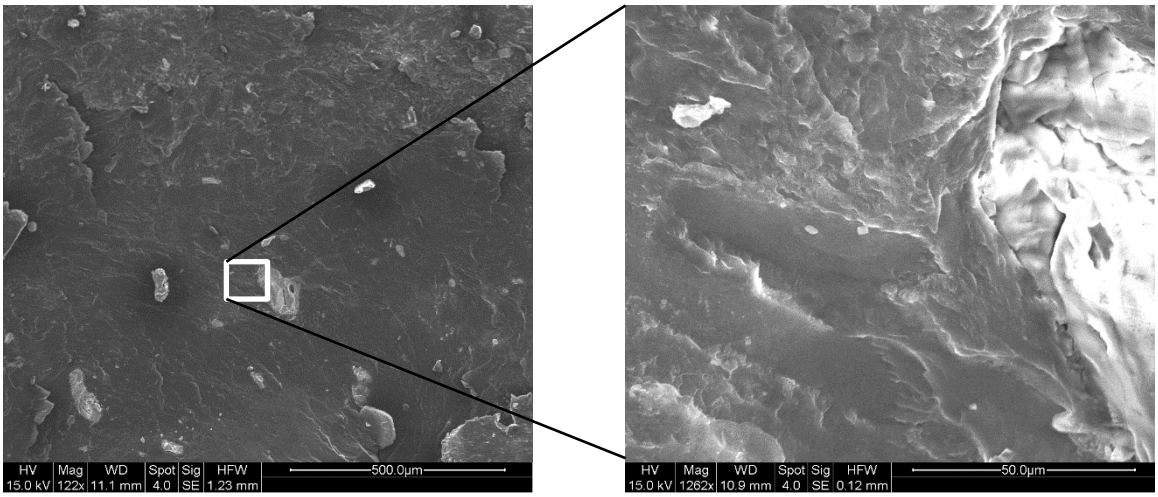

Figure 24: SEM Images of 0.50wt% rGO

Commentary on the dispersion of rGO is more difficult as the contrast between these additive particles and DB matrix is more subtle at the higher magnification; usage of back scattering electron imagery did not provide greater contrast. In other images taken of 0.50wt% rGO, particles were not confidently identified.

Carboxyl FGS

Much like the prepared graphite particles, the prepared isolated carboxyl particles experience some conglomeration during the SEM sample preparation, as seen in Figure 25, due to the vaporization of the acetone solvent in which it was sonicated. Imagery of the previous materials indicate that this feature is not representative of the additive in the processed propellant mixes, though it does give an indication that this material may have a tendency to agglomerate. Figure 25 does display standalone particles on the order of 5μm in size with larger particles approximately 20μm in length.

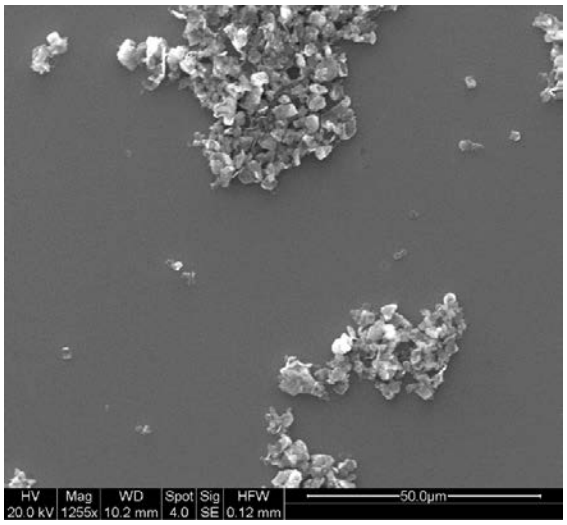

Figure 25: SEM Image of Carboxyl FGS particles

The images of the particle size and distribution of 1.00wt% Carboxyl FGS can be seen in Figure 26. The scanning electron imaging setting makes the distinction between sample surface topology and additive material difficult for the less magnified image on the left; however, the particles are more visible for the 2000x magnification image to the right. In the higher magnification image, the white specks are the Carboxyl additive. From this image, it is clear that the particle sizes are quite small, with the largest in this view being no more than 20µm in length, and some smaller particles apparent. This matches very well with the particles imaged in Figure 25.

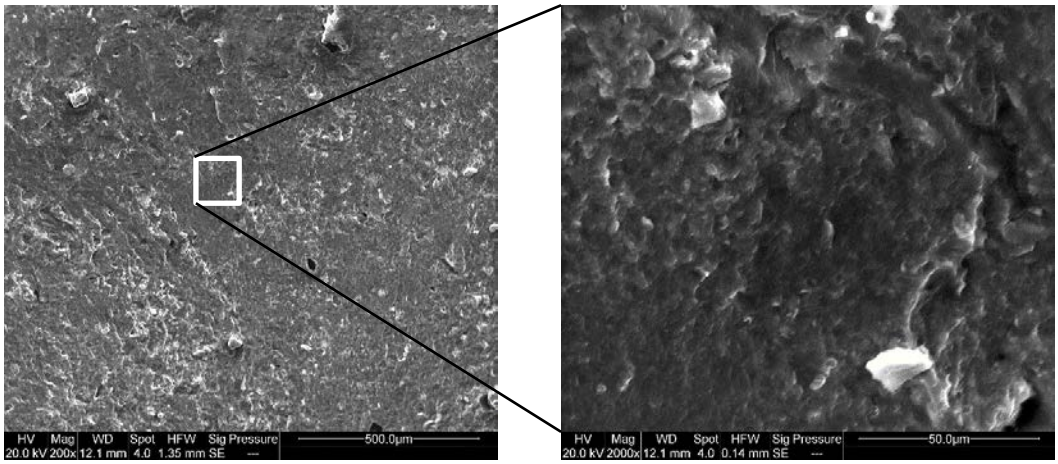

Figure 26: SEM Images of 1.00wt% Carboxyl FGS

Though the particles do not appear to be densely grouped, there does appear to be portions of the observed sample that do not contain any additive material. This is relatively consistent with the other imaged areas of this additive material and concentration. The apparent absence of additive particles may be due to the relatively poor contrast between the DB propellant and carbon additives as seen in many of the other images of propellant admixtures.

Chapter 5

Experimental Procedure

Optical Strand Burner

Propellant burning rates were evaluated by using an optically accessible strand burner located at the Kenneth K. Kuo High Pressure Combustion Lab (KHPCL) at Penn State. This apparatus, pictured in Figure 27, consists of a 4.2L chamber, which can be securely sealed to pressures up to 65.6MPa (9,500psi). The chamber contains a viewing port with a window consisting of two pieces of 3cm polycarbonate blocks. This window allows for unimpeded visual access to the test specimen and withstand the full pressure range of the chamber.

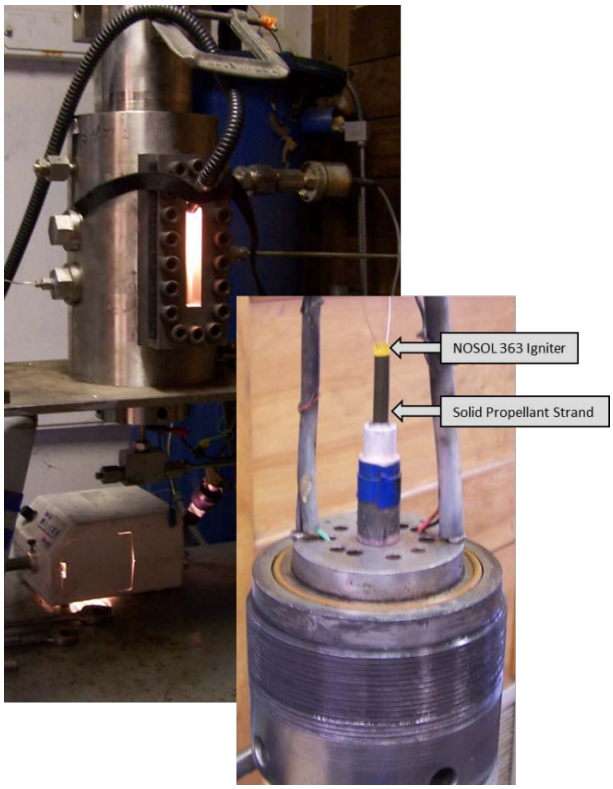

Figure 27: Strand burner set up

For this investigation, all tests were done at 27.6MPa (4,000psi) in an inert nitrogen environment. This pressure was selected as a representative pressure that is appropriate for real-world application environment of DB propellants, but does not require a large amount of resources for the large number of tests run. Additionally, the chamber has favorable optical properties at this pressure; smoke recirculation in the chamber does not block camera view. The pressure and nitrogen gas are provided by using a HYDRO PAC C30-20FX Gas Compressor to compress gas from a nitrogen cluster located on lab premises.

The rate at which the gas enters the test chamber is achieved manually by a series of hand valves. To further reduce the chances of smoke recirculation from blocking video recording, a light purge flow is sustained throughout the experiment. Balancing the incoming compressed nitrogen and the outflowing purge to maintain the target pressure is established before DAQ or camera begin recording. Chamber pressure is measured using a Setra Model 206 pressure transducer (visible in Figure 27). The transducer signal is sent to instruNet 3.6 Data Acquisition system (DAQ) for data recording and a LabVIEW program used to monitor chamber conditions during experiments.

The sample strands, as described in the Pre-Test Preparation section, were placed into the holder, as seen in Figure 27, and secured by friction fitting. Strands were ignited by an electrically heated nichrome wire run through a small piece of NOSOL 363 solid propellant installed on the top surface as an ignition booster. The NOSOL igniter provides a uniform and reliable ignition of the top surface of the strand. 5VDC is applied across the wire to provide the power to heat the nichrome wire. This power is controlled by a toggle switch on the strand burner control panel and is recorded by the DAQ system.

Video recordings of the burning propellant are captured by a digital camera (iDS USB3 UI-325xML-C) mounted on a tripod directly facing into the viewing port of the strand burner

chamber. Video from this camera was recorded and saved using the camera manufacturer accompanying software (iDS uEye Cockpit 4.80). The recording settings are displayed in Table 6.

Table 6: Video Recording Setting

Gain	x1, No Boost
Pixel Clock	128 MHz
Frame rate	120.09 fps
Exposure	.020 ms
JPEG quality	90%

The combustion of the DB propellant is incredibly bright and easily oversaturated the initial recorded videos. The exposure rate is the smallest that the software could provide and was still insufficient to fix the oversaturation issue. To compensate, a series of two neutral density filters (B+W filter ND0.9[103] and Hoya NDx4) were applied in front of the camera lens. The set of filters reduced the captured light to 1/32 of the light emitted by the flame. This reduction in light made it possible to clearly see and track the flame front as it regressed down the propellant strand.

Data Analysis

The collected video is analyzed with image processing software (ImageJ) to track the regression of the burn surface. Each frame of the video, during the burning of the propellant, is marked with a point at the burning surface. The points selected are representative of the burning surface as a perfectly flat regression is not very common. Usually other features (slight slants, peaks, divots) present on the surface make it necessary to select a point representative of the whole surface, in this investigation, an estimate of the average height of the burning surface.

Snapshots of this procedure can be seen in Figure 28. The pixel location and frame of each point of all frames in the video are saved for further regression deduction.

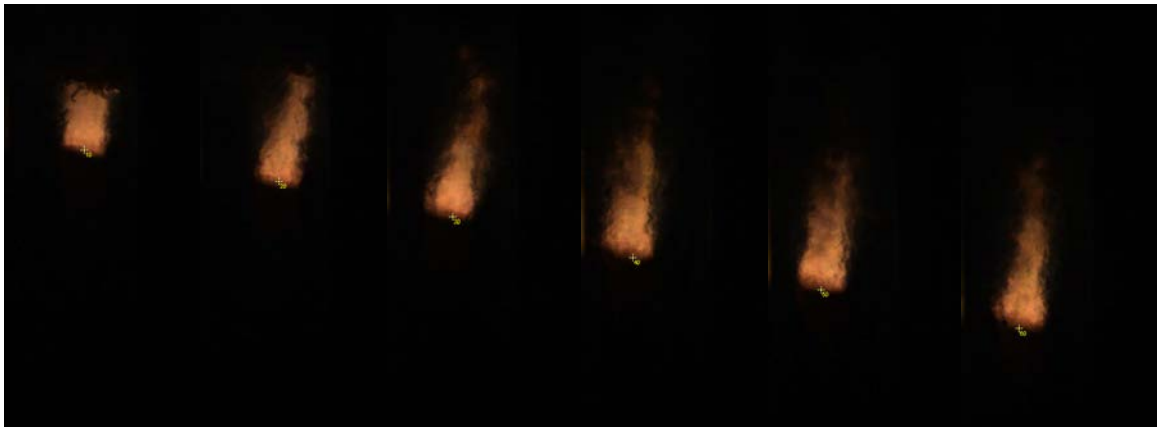

Figure 28: Video snap shot of burning regression

A script file was written to take the raw data collected from the DAQ and the data points from the video analysis to compute the burning rate of the strand and the pressure of the chamber during the experiment. This script was written for the use in both MATLAB and Octave, and can be viewed in Appendix C. Initially, the ImageJ regression data are imported into an array and converted from pixel location and frame to millimeters and seconds, respectively, using the camera scale and video frame rate. The converted arrays for location and time are plotted against each other and linearly fitted. The slope of this fitted curve corresponds to the burning rate of the propellant. A plot of these data points (blue circles) and the fitted curve (dotted red line) for a test of processed DB propellant with no additive can be seen in Figure 29. This method of calculating the burning rate of each strands leads to an average measurement uncertainty of ±5%.

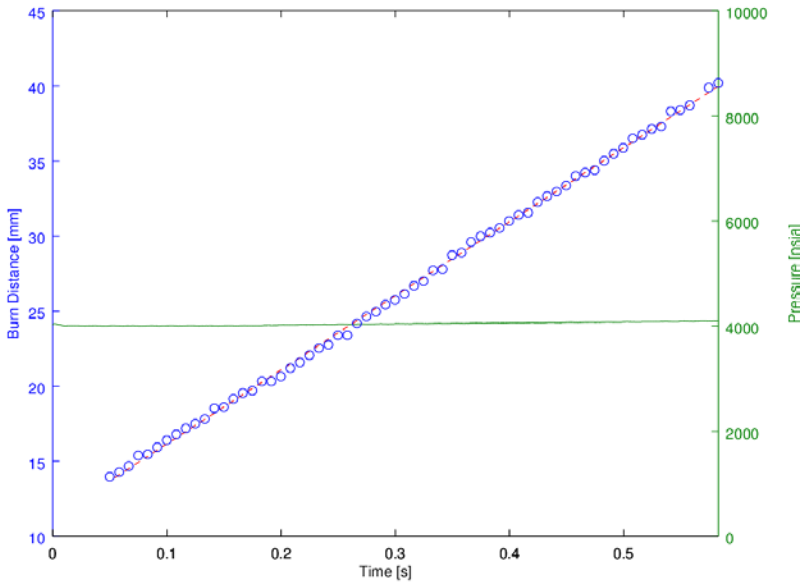

Figure 29: Regression Analysis Plot

Also plotted with the burn regression data, as seen in Figure 29, is the chamber pressure during the timespan of the experiment. This observation serves as a check on the value and behavior of the pressure profile throughout the test. The purge flow in the chamber is manually established to allow for a constant pressure; however, some increase is inevitable throughout the test due to gas generation during propellant combustion. The utilized process for establishing pressure leads to a standard deviation of the pressure magnitude during the experiment to be around 0.1%.

The propellant burning rate, burning rate uncertainty, chamber pressure, standard deviation of chamber pressure, as well as, the density for each tested strand is recorded and collected in a large spreadsheet. The evaluation and compilation of the burning rate data for the tested additive materials and concentration are depicted and discussed in the following chapter.

Chapter 6

Results and Discussion

Burning rate

The collection of all the data sets, including burning rate and density, for all additive materials and concentration allows for a multitude of quantitative analysis and comparison of propellant performance against additive materials, concentration and batches. Evaluating the behavior of a particular additive material and concentration from batch-to-batch is insightful for investigating any measurement biases or errors that may be present, or the effectiveness of implementing new process techniques as seen in Figure 7. The batch-to-batch does not give insight in regards to the relative behavior of the effects on the various additive materials or the sensitivity to additive concentration.

A useful means in comparing data for each of the additive materials and concentrations against one another is utilizing a simple bar chart. Figure 30 displays the values of the average burning rates for the tested additive materials and concentration. The error bars displayed are either one standard deviation of the data points within each set or the measurement uncertainty, whichever is greater.

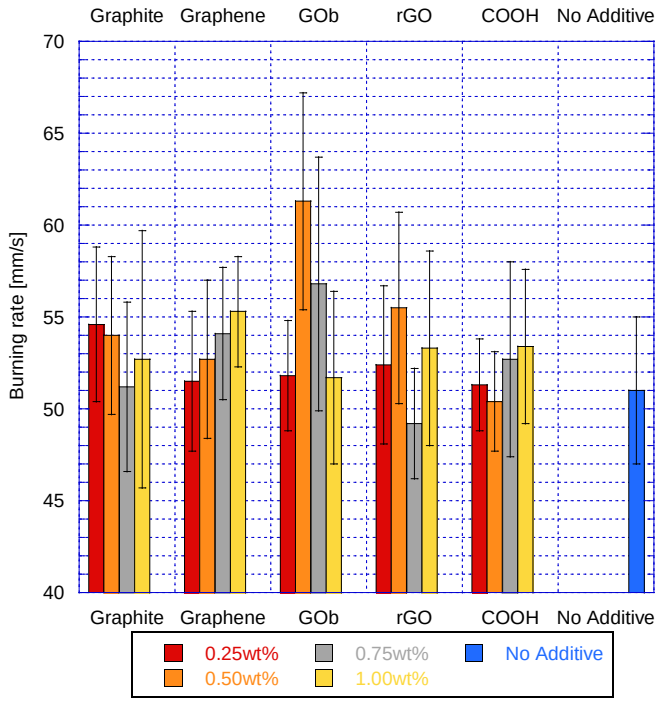

Figure 30: Burning rate comparison of additive materials in DB propellant

From the comparison in Figure 30, most of the observed additive materials and concentrations show increased average burning rate as compared the DB propellant with no additive material. This may suggest that some of the fundamental property changes of introducing a carbon powder additive into the propellant boosts the performance of the DB propellant. Without fully characterizing the materials, it is unknown which property change or combination of property changes, such as thermal conductivity, absorptivity or particle surface area, contributes to this behavior. The exception to this observation is 0.75wt% rGO.

The behavior of 0.75wt% rGO is unexpected, as it does not follow any trend in concentration sensitivity. Other additive materials demonstrate some loosely continuous trend in the average burning rate with additive concentration. Graphite demonstrates average burning rate decreases as concentration increases. With no local maximum visible, this could mean further increase in burning rate may be possible at lower concentrations of graphite. The decrease in average burning rate with increasing concentration may be an indication that relative abundance

of carbon is removing energy from the combustion as a source of fuel and thus reducing the burning rate.

Graphene demonstrates a mirror trend, where 0.25wt% seems to suggest little to no change in the average burning rate, which could indicate no effect on the DB baseline, and average burning rate increases with increasing concentration. Similar to graphite, no local maximum is apparent in Figure 30, which could indicated a greater average burning rate could be achieved at a higher concentration of graphene. The sensitivity behavior of the carboxyl (COOH in Figure 30) is similar to that of graphene. These trends are similar to that observed by Zhang[32] with the effect of concentration of GO on the burning rate of nitrocellulose film.

Unlike the other additive materials, GOb shows a definite local maximum in average burning rate at a concentration around 0.50wt%. Another distinguishing behavior is the steepness of the trend, suggesting that the performance of the DB propellant with this additive material is very sensitive to the concentration.

The relatively large error ranges, mostly driven by scatter in measured burning rates, makes it difficult to assert definite statements on behaviors or trends. However, a more confident assertion can be made when a data set for a particular additive material and concentration exhibit statistically significant difference in a value as compared to the DB propellant with no additive. In this investigation, a material is said to be statistically significant compared to the DB baseline if the error bar ranges of the material and DB baseline do not overlap. As can be seen in Figure 30, the lower limit of the error bar range of 0.50wt% GOb is greater than the upper limit of the error bar range of DB with no additive. This gives much greater confidence that 0.50wt% GOb burns at a faster rate than the DB baseline.

Other noteworthy materials and concentrations that appear to exhibit enhanced burning rate behavior are 0.75wt% GOb and 0.50wt% rGO. These materials have an average burning rate that is greater than the upper limit of the neat DB baseline. Two different concentrations of GOb

are exhibiting some increase in burning rate over the neat DB baseline, which suggests this material is having an enhancement effect on the combustion DB.

An insightful way of evaluating the burning behavior of the various tested propellants is to normalize the linear burning rate by the density of each test strand yielding a mass burning rate. Density of a test strand is more susceptible to variability as a result of the lab scale production procedure. Figure 31 depicts the mass burning rate of the tested additive materials in concentration. Each material and concentration data set is a sub set of tests used in Figure 30. The data depicted in Figure 31 are only tests that had strand densities determined using a higher precision specific gravity bottle, while the data depicted in Figure 30 is any test that was subjected to ventilation during the drying process.

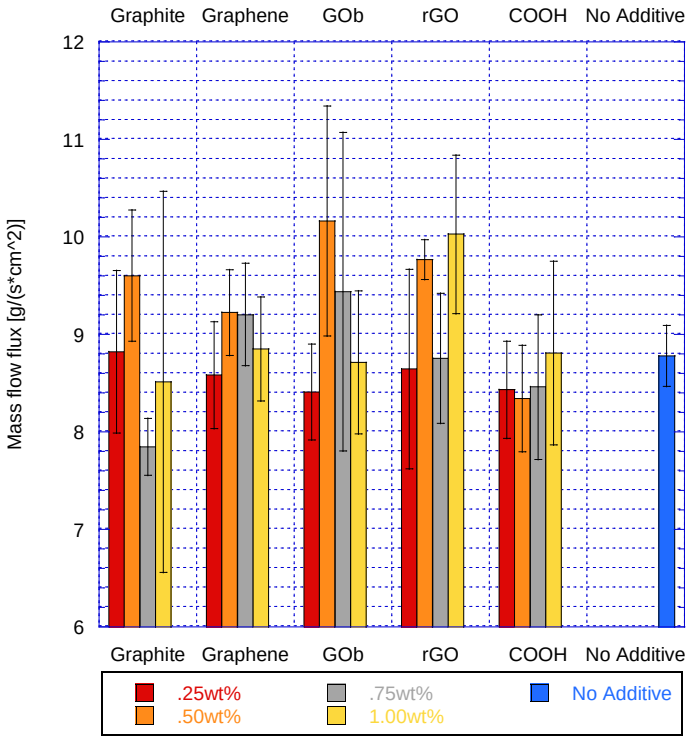

Figure 31: Mass burning rate comparison of additive materials in DB propellant

For the functionalized graphene additives, the relative behaviors of the concentrations in terms of ‘greater/less than’ are for the most part conserved, which is beneficial in understanding

the effect of concentration of an additive material on the DB propellant. GOb appears to have a maximum performance at a concentration between 0.50 and 0.75wt%. Tested strands mixed with carboxyl (COOH) FGS exhibit a higher mass burning rate at a concentration at or potentially greater than 1.00wt%. At the moment, rGO tested materials appear to be bimodal at 0.50 and 1.00wt%.

As stated earlier, the current mass burning rate data set is smaller than that of burning rate data. More importantly, some of the data sets are represented by only one extruded batch; this included 0.75wt% graphite, 0.25, 0.75 & 1.00wt% graphene, 1.00wt% GOb, and all concentrations of rGO. Test strands from a given batch are expected, but not necessarily, to behave similarly and can give a false impression of the true behavior of the material.

With that in mind, some interesting observations can still be pulled from Figure 31. 0.50wt% GOb maintains its status as the greatest increase in burning behavior as compared to the DB baseline. Unlike burning rate, the mass burning rate 0.50wt% GOb admixes cannot be said to be statistically significant as the error bar ranges of 0.50wt% GOb and neat DB overlap. 0.50wt% and 1.00wt% rGO and 0.75wt% graphite do exhibit statistically significant difference in mass burning rate compared to the neat DB.

The 0.50 and 1.00wt% rGO admixes exhibit an increase in mass burning rate. Though both of these materials and concentrations would benefit from additional batches of material for comparison to be more certain of burning behavior, 0.50wt% rGO does exhibit a burning rate that is greater than the upper error limit of neat DB, as seen in Figure 30. These observations made together would suggest that some enhancement in burning behavior of the DB propellant is achieved with 0.50wt% rGO.

Interestingly, 0.75wt% graphite appears to inhibit the mass burning rate of the DB propellant. As mentioned before, more test batches of this material are needed to lend greater certainty to this observation. By observing the similarity in burning rate between 0.75wt%

graphite and neat DB in Figure 30, it seems that the reduction in mass burning rate may be driven from a relatively lower strand density of 0.75wt% graphite compared to the DB baseline.

Density

With a precise way of measuring strand density, it is insightful to compare the average measured densities of all the tested materials and concentrations. Additionally, observing any trends in density across the different materials and concentrations may give a better understanding of the values and trends observed in mass burning rate, as seen in Figure 31. The data set used in the comparison of strand density is slightly larger than that of burning rate data. This is due to the simple fact that all extruded and prepped strands had density measurements made although not all test strands yielded useable data.

Figure 32 depicts the comparison of the average measured density for each tested material and concentration. The error bar ranges in this figure are one standard deviation of each data set. The use of the Hubbard specific gravity bottle has dropped the measurement on certainty of density to a value that is much less than any of the data set deviations.

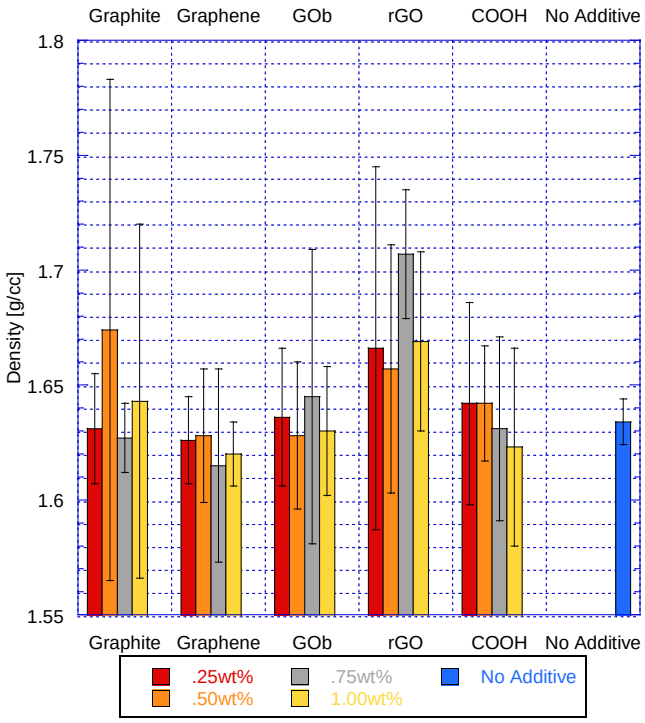

Figure 32: Density comparison of additive materials in DB propellant

Overall graphite, graphene, GOb additives at all the tested concentrations exhibit lower densities compared to the DB baseline. The carboxyl (COOH) FGS additive appears to exhibit little to no change density as compared the DB baseline. The scatter in each of the data sets makes statements on the effect of additive material on strand density uncertain.

However, 0.75wt% rGO exhibits statistically significant increase in density compared to the DB baseline. The other concentrations of rGO exhibit average strand density greater than the upper error limit of the DB with no additive. This may suggest the rGO additive does lead to the extrusion and drying of more dense material. A likely possibility to this behavior is the size of the additive particles. This could mean that the additive can be mixed within the DB matrix, increasing mass, without leading to an increase in volume.

As mentioned in Chapter 4, comparing the measured strand densities to the calculated theoretical densities in Table 5 will give a qualitative and quantitative insight on the relative prevalence of micro-voids and occlusions within strands, and what affect different additives may

have on that behavior. This comparison was done by subtracting the theoretical values in Table 5 from the measured values displayed in Figure 32. A positive difference suggests a propellant admixture was able to achieve a density greater than the theoretical. A negative difference may suggest a tendency of a propellant admixture to develop internal micro-voids or occlusions during the extrusion and drying process. The results of this subtraction is displayed in Figure 33. The error ranges in this comparison is one standard deviation in the average, measured, strand density of each additive material and concentration.

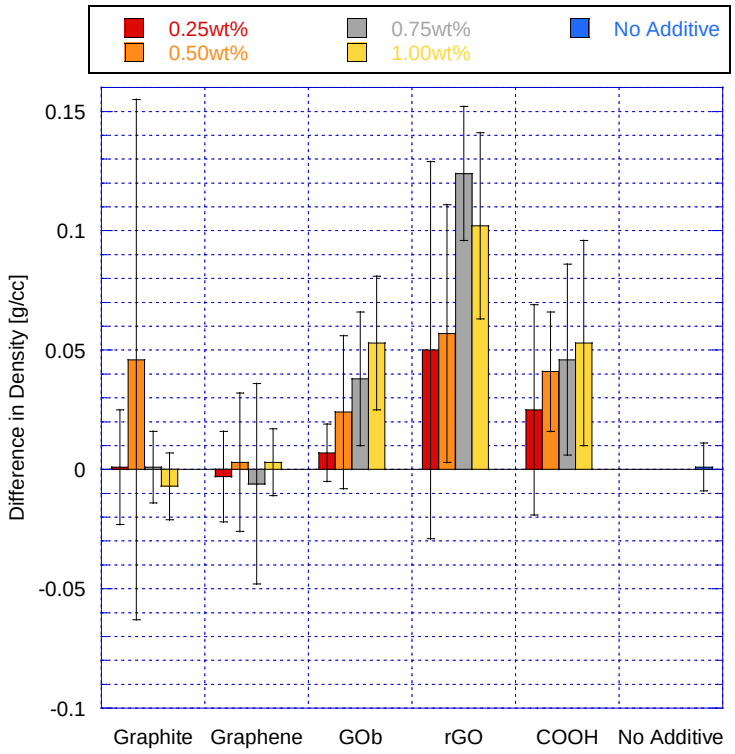

Figure 33: Comparison of Theoretical and Measured Density Values

The relatively large error ranges makes it difficult to come to make statements on the possible presence of voids in propellant strands with much certainty. What can be said is that no additive material or concentration produced exhibits statistically significant lower density as compared to the respective theoretical density. This statement seems to validate that the process established in extruding and drying propellants strands are not leading test materials riddled with

internal voids and occlusions. The three propellant admixtures that exhibit average strand densities less than the theoretical deviate from the theoretical value by less than 1%.

Several additive materials and concentrations exhibit a measured density greater than the theoretical value by a statistically significant amount: including 0.75 & 1.00wt% GOb, 0.50, 0.75 & 1.00wt% rGO, 0.50, 0.75 % 1.00wt% Carboxyl FGS. This behavior could suggest that the additive particles are small enough to slip within the interstitial spaces of the DB matrix. The particles images viewed in a previous section do demonstrate the potential for very fine particles to be homogenously dispersed in the DB propellant. If the processed DB propellant contains sufficient number and sized interstitial spaces within the matrix, additive particles could fill these spaces; adding mass without increasing the volume would lead to a larger density. Alternatively, the FGS may present a chemical change in the admixtures, in which the functionalized groups exert some form of attraction between the FGS and DB material leading to a denser substance overall.

Outlier Analysis

The large variability in data seen in burning rate and density data may be driven by the presence of outliers within data sets. Small data sets have prevented this analysis in the past, as it was felt that statistical analysis for outliers would be inappropriate. All of the small data set analysis methods are based on the assumption that the collected data follow a normal distribution about the true mean value, in this case burning rate. When data sets are too small, this assumption can be difficult to validate.

Dixon Q Test

This is a simple test more utilized in chemistry[33]. Unlike the other tests that will be discussed, the Dixon test evaluates the presence of an outlier by the ratio of the relative distance between two data points (sorted from lowest to highest magnitude) to the total range in values, depicted in Equation 5.

$$Q_i = \frac{x_n - x_{n-1}}{x_{max} - x_{min}} \quad (5)$$

If the value of Q is greater than the critical value for the desired confidence level, this test suggests there is an outlier present in the data set. The critical values of Q for various confidence levels is available in many statistical textbook and other literatures[34]. This test is very basic and easy to perform; additionally, this analysis holds for data sets as small as three data points. Using only the difference between values, information about the behavior of the data set as a whole is not considered. This test would best be served as validation for another more stringent method.

Grubb's Test

The Grubb's test stands as one of the most common methods for evaluating the presence of an outlier in a data set. This method relies more on the statistical behavior of the whole data set rather than relative differences in values[35]. As stated above, this method assumes that only one outlier exists in a normally distributed data set. For this reason, the Grubb's test utilizes the Student-t distribution and normalization. Unlike the modified Thompson Tau test that will be described below, the critical value for the variable G is based on a Student t value, as shown in Equation 6, based on both the confidence level and sample size. With other utilized parameters like the sample standard deviation and sample size, this method grants more variability of samples size which leads to its more frequent use in experimental data analysis.

$$G = \frac{max|x_i - \bar{x}|}{s} \quad (6)$$

$$G > \frac{n-1}{\sqrt{n}} \sqrt{\frac{t^2_{\frac{\alpha}{2N},n-2}}{n-2+t^2_{\frac{\alpha}{2N},n-2}}} \quad (7)$$

Equation 7 must be met for a data point to be considered an outlier.

Modified Thompson-Tau Test

The modified Thompson-Tau test is nearly identical to Grubbs' test for outlier analysis. The primary difference is the value of the critical Student t value. Whereas Grubb's test considers confidence level as well as sample size in the selection of the critical Student t value, the modified Thompson Tau test only considered the confidence level, as seen in Equation 8. Overall, this leads to lower outlier thresholds as compared to the Grubbs' test. Another distinction between the two tests is that the modified Thompson Tau test can detect the existence of multiple outliers as each value of δ is evaluated against the outlier threshold value, as expressed in Equation 8.

$$\delta_i = \frac{|x_i - \bar{x}|}{s} \quad (8)$$

$$\delta_i > \frac{n-1}{\sqrt{n}} \sqrt{\frac{t^2_{\frac{\alpha}{2},n-2}}{n-2+t^2_{\frac{\alpha}{2},n-2}}} \quad (9)$$

Evaluation of Data Sets

As there is currently no absolute agreement on a definitive outlier test, all three of the explored outlier analysis methods were utilized in the evaluation of the current burning rate data sets. A script file was created which takes the burning rate values of a given additive material and

concentration and evaluates the set with the above methods and returns if there is a data point that meets the respective criteria and which value that is.

For a data point to be considered an outlier and removed from the calculations and comparisons of this investigation, it must be recognized as an outlier by at least two of the methods. Requiring agreement of two methods to indicate the presence of an outlier serves to validate that a data point can confidently be considered an outlier, and can be removed from the data set. If a data point is recognized as an outlier by only one analysis method, the data set and data points will be investigated further with methods including re-evaluation of the regression videos, considered from extrusion in the next batch of materials or analyzed for other methods that may have given rise to deviating data point.

A standard level of certainty for engineering systems is generally taken to be 95% which corresponds to $\alpha=0.05$. This confidence level will be used for the evaluation of the burning rate data sets for the evaluation of outliers. At this level of confidence and the methods described above, the following additive materials and concentrations for burning rate and density measurements that exceed the outlier are as followed:

- Burning rate
    - Single test recognition (modified Thompson Tau test)
        - DB with no additive
        - 1.00wt% graphene
        - 0.25, 0.75 & 1.00wt% GOb
        - 0.25, 0.75 & 1.00wt% COOH
    - Multiple test recognition
        - N/A
- Density
    - Single test recognition (modified Thompson Tau test)
        - 0.50wt% graphite
        - 0.50wt% graphene
        - 0.50wt% GOb
        - 0.75wt% rGO
        - 0.25, 0.50 & 1.00wt% COOH
    - Multiple test recognition
        - 1.00wt% graphite
        - 0.25, 0.75wt% GOb

It should be mentioned that the only test that recognized the presence of the outliers in a dataset is the modified Thompson Tau test. As observed previously, the definition of the outlier threshold level of the modified Thompson Tau test leads to a lower value. This would suggest that this test would recognize outliers more readily as compared to the Grubbs' test.

The listed tests recognized by the modified Thompson Tau test are subjected to additional scrutiny and evaluation to get a better understanding of the existence of those deviant values. No dataset of burning rate tests was recognized to contain an outlier by more than one evaluation method. This means no points will be removed from the analysis, and the results of Figure 30 remain unchanged.

Unlike burning rate data points, the measured density data points recognized by a single test cannot be subject to re-analysis as the strands have been burned. Producing additional material to bolster these data sets was not able to be achieved within the remaining time of this investigation. Also in contrast to the burning rate data, three data points that were recognized by two or more outlier tests were removed from analysis. The resulting comparison of densities is displayed in Figure 34.

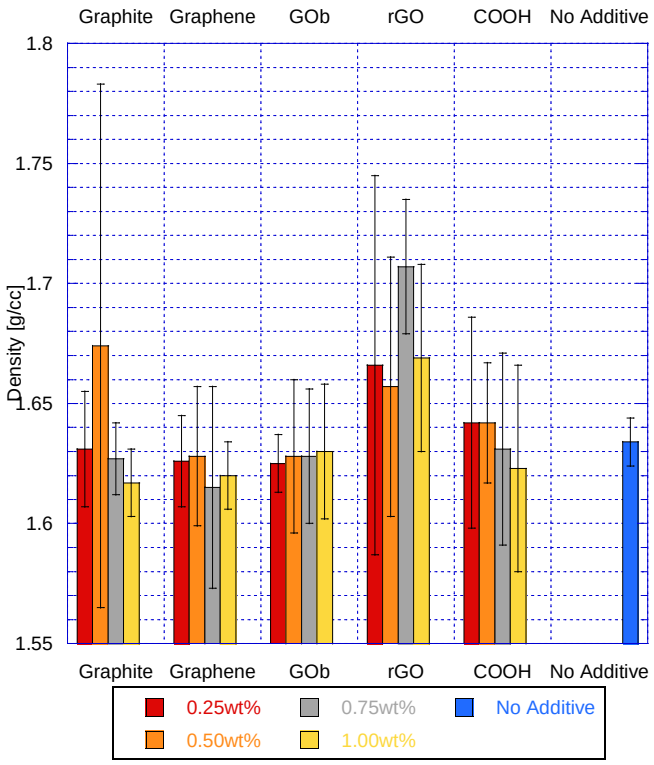

Figure 34: Density comparison with outliers removed

Significant scatter still exists in some of the materials and concentrations. These involve the data sets with an outlier recognized by the modified Thompson-Tau test but no other. Overall, the previously observed relative behaviors of additive material and concentration are maintained when the outliers are removed.

As the value of mass burning rate is dependent on the value density and linear burning rate, the results of outlier analysis of both those parameters greatly affect mass burning rate data sets. If an outlier is identified and eliminated from either the data set for linear burning rate or density, the corresponding mass burning rate value must also be removed from analysis. No linear burning rate results were recognized as outliers and thus no changes in mass burning rate was made. Three data points, identified above, of density were recognized and removed from analysis; the corresponding mass burning rate data point was removed from analysis. The resulting comparison is displayed in Figure 35.

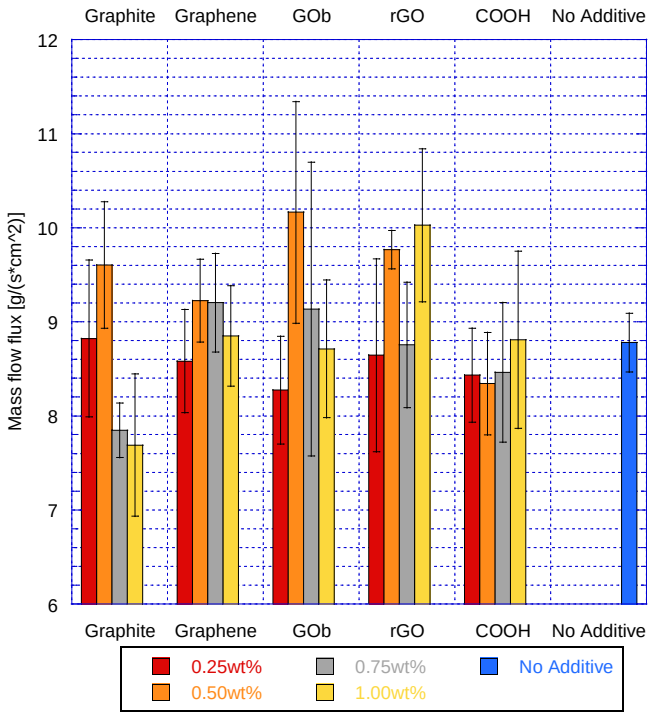

Figure 35: Mass burning rate comparison with outliers removed

The most significant change from the full data set is the reduction in average mass burning rate of 1.00wt% graphite and its error range. This change leads to what appears as a great sensitivity to concentration of graphite additive. 0.25wt% graphite exhibits an average mass burning rate very similar to that of DB with no additive. 0.50wt% graphite exhibits enhanced mass burning rate, with an average above the upper error limit, but cannot be said to be statistically significant. 0.75wt% and 1.00wt% graphite show a drastic reduction in mass burning rate to averages below that of the DB baseline, and can be said to be statistically significant as there is no overlap with the error range of the DB baseline. The rest of the relative behaviors remain the same and the previous observations and comments made above still apply.

Thermal Decomposition

TA Instruments provides a publicly available data analysis program for thorough and precise evaluation of all collected data. Using this software and the expertise of the MCL lab manager for thermal analysis equipment, collected data gives insight on the fundamental decomposition behaviors and interactions between the DB propellant and the various additive materials tested. Because each experimental run, including setup and cleanup, is roughly two hours, and the fact that access to the equipment relatively late in the research process, tests were taken of all additive materials at only one concentration level, 0.50wt%.

Before the sample materials were tested, results from available literature was used to develop the heat profile for tests, as previously mentioned. The results of Fiamengo's work[30] of thermal decomposition of double base propellants served as a great reference for the expected behavior of the propellants, and ensured that the materials would not be too hazardous for use in the TGA machine. In the paper, several formulations of double base and single base propellants were used in an attempt to understand the effects of the amount of nitroglycerin on mass loss during gradual thermal decomposition. The results for their composition of a single base, nitrocellulose (NC) propellant and a double base propellant with a formulation most similar to that used in this investigation are displayed in Figure 36. This figure plots the relative mass loss (instantaneous mass divided by the initial mass) of the samples, including the data obtained in this investigation, against the temperature of the sample.

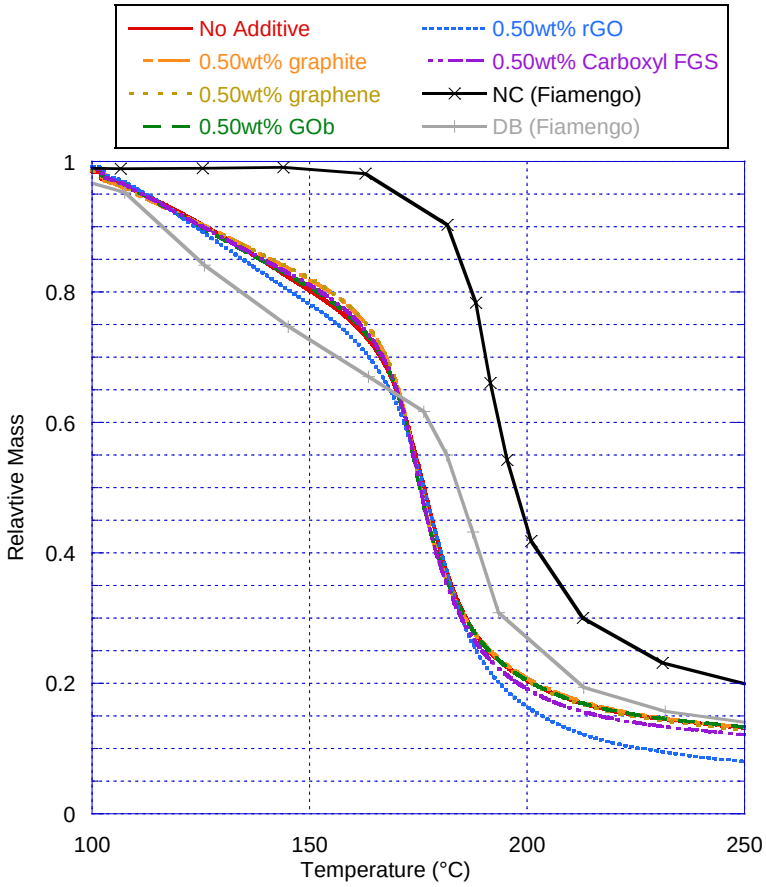

Figure 36: TGA Data comparison to literature

The comparison to literature results is done as another means of validating that the obtained results are capturing truly representative behavior. The M9 with no additive, shown by the solid red line, exhibits many of the same features as Fiamengo's decomposition curve for a 'typical double base propellant.' There is a gradual mass loss of the propellant that then experience a much more rapid rate of decay around 170 to 180°C, and then again levels off with nearly no mass loss beyond 250°C. The similarity in these two curves, DB (Fiamengo) and No Additive, is reassuring that observed behavior is indicative of double base propellants in general. The difference in these curves are a result of different compositions. This is because all the compositions utilized in Fiamengo's work contain much larger amounts (weight percentage) of stabilizers and plasticizers than most commercially used double base propellants, especially

compared to the formulation used in this investigation; 8wt% of dinitrotoluene in the Fiamengo compositions compared to 0.75wt% diphenylamine in the DB used in this investigation. So much stabilizer was used in the Fiamengo study in order to slow and regulate decomposition and better analyze differences between propellants in the attempt to determine NG level based on thermal characterization alone.

In regards to the collected data as displayed in Figure 36, there is remarkably similarity in the decomposition behavior of each of the propellant admixtures to the baseline propellant. Each mixture exhibits a very gradual decay from 25°C to 100°C (not shown in Figure 36). Around 100°C the propellants exhibit a marked increase in the rate of decomposition. According to Fiamengo, this change in behavior is related to the vaporization and decomposition of the NG in the double base propellant. The greatest rate of decomposition, uniformly experienced by the propellant admixtures, occurs around 160°C, which corresponds to the onset of NC decomposition as evident in the NC (Fiamengo) curve in Figure 36. With decomposition features and behavior more indicative of the NC and NG trends and recognizing that all the tested additive material propellant mixtures seemingly exhibit identical behavior, there is little indication that the tested graphite and graphene materials significantly influence the decomposition behavior of the baseline DB propellant. This is only a qualitative observation on the mass loss experienced by each of the propellant mixtures. Greater insight is possible when quantitatively comparing features of the change in mass with respect to temperature of a sample and the heat flow from the sample.

The continuous and linear nature of the of the TGA-DSC curves makes it possible to appropriately use the derivative mass loss and energy flow data for these samples. The 2mg samples were able to be better captured by the thermocouples and mass balance of the instrument. Table 7 contains the characteristic values (maximums) for the derivative mass loss with respect to temperature, specific heat flow, and the temperature at which these values occur.

Table 7: Characteristic TGA and DSC Values

Material	Max Deriv. Mass Loss (%/°C)	Temperature of Max Deriv. Mass Loss (°C)	Peak Heat Flow (W/g)	Temperature of Peak Heat Flow (°C)
No Additive	2.551	176.36	6.077	178.7
0.50wt% graphite	2.979	174.43	7.035	175.6
0.50wt% graphene	2.813	174.41	7.437	175.7
0.50wt% GOb	2.796	174.60	5.408	175.3
0.50wt% rGO	2.338	178.21	7.372	178.9
0.50wt% COOH	2.878	174.88	6.406	176.2

The temperature at which these peaks occur correlate strongly to the temperature of maximum rate of heat loss. The difference in the characteristic temperatures is likely related to the response times of the mass balance and thermocouple, as the thermocouple experiences delay due to conduction through the sample crucible.

For all cases of additive material, the maximum value for the derivative mass loss with respect to temperature is greater than that of the DB baseline with exception of the 0.50wt% rGO mixture. This increase, ~10% greater than the baseline across the additive materials, suggests that the introduction of a carbon material into the DB matrix. The values of maximum derivative mass loss for graphite, graphene and carboxyl FGS are the greatest of the additive materials. What is interesting about this observation is that these additives are the most stable of the tested additive materials, as discussed in a previous section. This would suggest that the slight increase in decomposition of the propellant mixtures is not directly caused by the decomposition of the additive material but could potentially indicate some catalytic activity between the graphite/graphene and the DB propellant. This statement is further supported by observing that the graphite and graphene propellant admixtures also exhibit the large increases in the specific heat flow from sample.

The 0.50wt% GOb propellant mixture exhibits the smallest increase in the maximum derivative mass loss, yet the additive material exhibits a greater degree of decomposition. Though it is an increase over the baseline, there is no evidence of the decomposition risks mentioned in

literature. This is especially evident when observing the peak specific heat flow from the GOb sample. The GOb propellant mixture is the only sample that exhibits a peak specific heat flow less than that of the baseline propellant.

The 0.50wt% rGO propellant mixture exhibits a distinctly different behavior when observing the temperatures of maximum derivative relative mass loss and peak heat flow. All other additive materials exhibit a temperature of maximum derivative mass loss around 174°C whereas the rGO mixture is roughly at 178°C. As will be discussed in a subsequent section, an offset in these characteristic temperatures to a value greater than the baseline maybe an indication of increased stability. This observation is slightly contrasted by observing the greater decomposition exhibited by this mixture in Figure 36 and that this mixture also exhibits one of the largest value for peak heat flow.

Thermal Stability

When dealing with propellant mixtures it is imperative to understand of the changes in composition lead to stability and compatibility issues. Statements have been made above about qualitative features that may indicate the relative stability of a propellant mixture compared to the DB baseline. Several quantitative assessments exist to evaluate the thermal stability and component compatibility. An open and international standard for this is published by NATO Military Agency for Standardization's Standardization Agreement (STANAG) 4147[21]. This document lays out a number of methods to evaluate the chemical compatibility for ammunition. Two of these tests can be performed from the data collected and discussed above: Test 3A and Test 4.

STANAG 4147 Test 3A: Dynamic TGA

Test 3A is the source of the testing procedures that has been used in this investigation and laid out in a previous section. The criteria for stability is based on the difference between the observed decomposition of the propellant mixture and the calculated decomposition for the propellant mixture. The DB propellant and each of the additive powders are subjected to the same testing procedures to derive a calculated mass loss for the propellant mixture. The decomposition experienced by the propellant mixture cannot exceed 4% of the individual decomposition of the mixture components. The equations to calculating the observed, calculated and difference, %Δ, are displayed below; %m is the relative mass measured by the TGA-DSC equipment, and Y (for the samples used Y_{DB}=0.995 and $Y_{additive}$=0.005) is the mass fraction of the mixture components. A graphical representation of these calculations, using the 0.50wt% Carboxyl propellant mixture, are shown in Figure 37.

$$\boldsymbol{observed} = \mathbf{100} - \%\boldsymbol{m_{mix}} \tag{10}$$

$$\boldsymbol{calculated} = (\mathbf{100} - \%\boldsymbol{m_{DB}}) * \boldsymbol{Y_{DB}} + (\mathbf{100} - \%\boldsymbol{m_{additive}}) * \boldsymbol{Y_{additive}} \tag{11}$$

$$\%\Delta = \boldsymbol{observed} - \boldsymbol{calculated} < \mathbf{4}\% \tag{12}$$

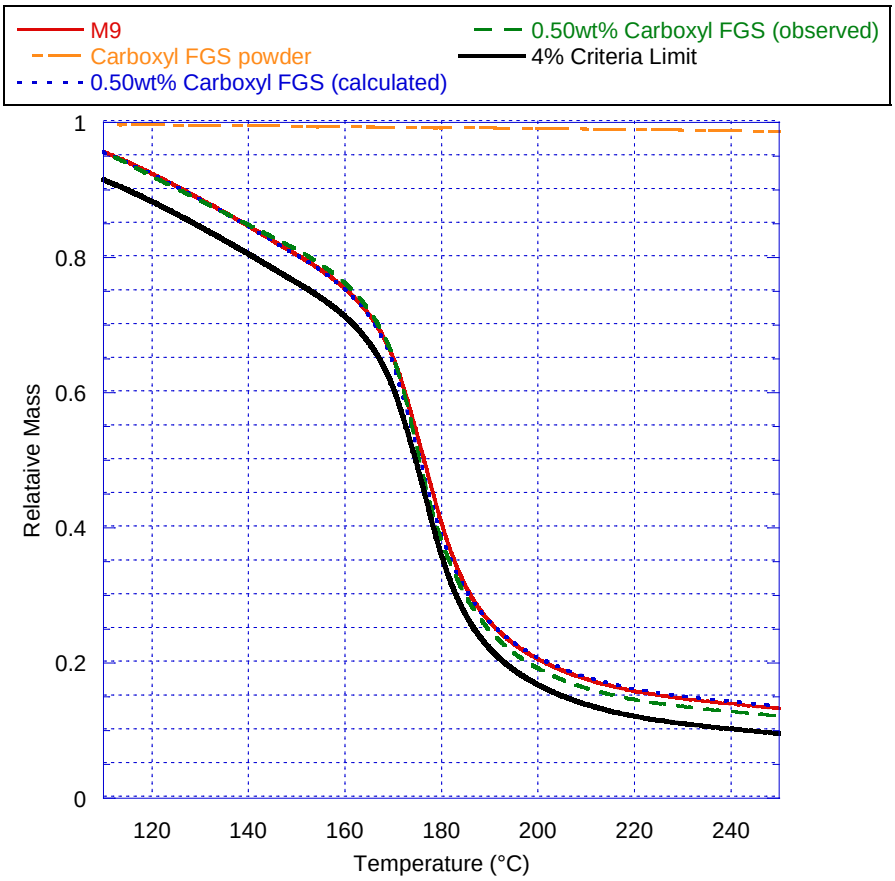

Figure 37: STANAG Test 3A Graphical Representation of 0.50wt% Carboxyl FGS

The dotted blue line in Figure 37 is the calculated mass using the decomposition curves of the constituent components as calculated using Equation 11. The solid black line represents the 4% offset of the calculated decomposition of the propellant mixture and is the criteria limit for chemical compatibility for STANAG Test 3A. For a propellant mixture to be considered thermally stable, the observed decomposition cannot cross the limit. For the 0.50wt% Carboxyl FGS mixture, the observed decomposition never exceeds the 4% Criteria Limit and can confidently said to be stable and exhibit no chemical incompatibility between the DB propellant and the carboxyl FGS additive. To simplify the graphical representation in Figure 37 to include all tested additive materials, the results of Equation 12 for each of the propellant mixtures are plotted in Figure 38.

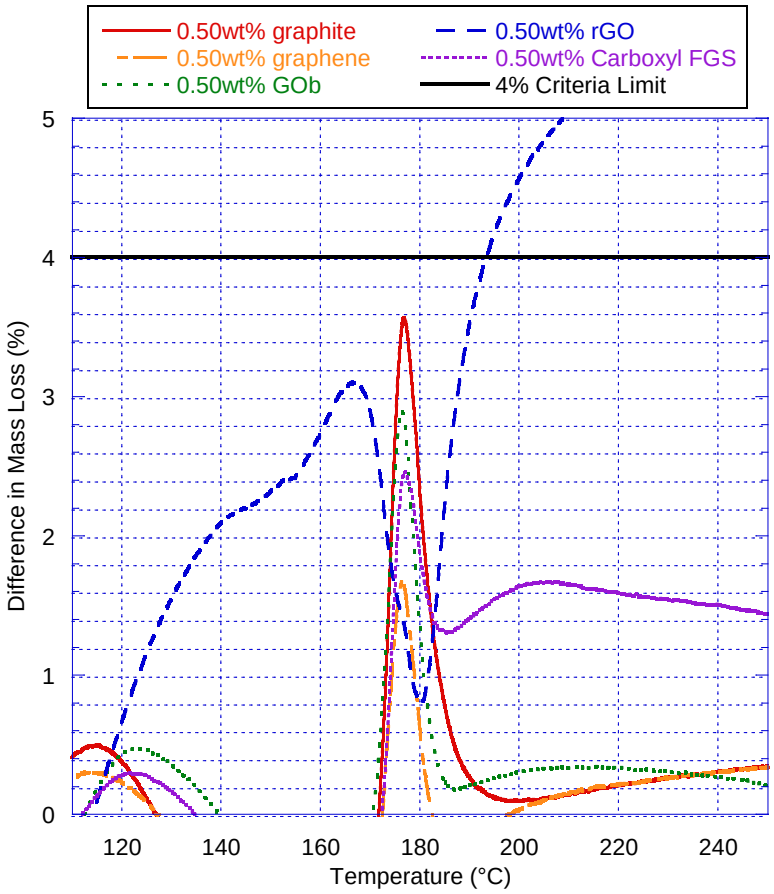

Figure 38: STANAG Test 3A Graphical Representation

As can be seen in Figure 38, only one of the additive materials cross the 4% chemical compatibility criteria limit as established in STANAG Test 3A. The maximum values for the graphite, graphene, GOb and Carboxyl FGS admixtures are securely below the threshold. These maximum values, indicated in Table 8, correspond to the temperature of the maximum derivative mass loss from the sample. With the calculation and evaluation done with the dynamic TGA data collected, it can be confidently stated that the tested propellant admixtures pass the criteria of STANAG 4147 Test 3A for chemical compatibility.

Table 8: Percent Mass Loss of Propellant Mixtures at Characteristic Temperature

Material	Temperature of Max Deriv. Mass Loss (°C)	%Δ
0.50wt% graphite	174.43	3.5
0.50wt% graphene	174.41	1.9

0.50wt% GOb	174.60	2.8
0.50wt% rGO	178.21	0.9
0.50wt% Carboxyl FGS	174.88	2.3

The statement made above may seem incorrect when noticing the behavior of the 0.50wt% rGO propellant mixture. This is the only additive material that crosses the 4% Criteria Limit in Figure 38, and has a noticeable greater decomposition than any other propellant mixture in Figure 36. Both of these observations would suggest that the propellant mixture containing the rGO additive exhibits chemical incompatibility to some degree. When analyzing the propellant admixture over the entire temperature range, it can be said there are signs of incompatibility; however, at the characteristic temperature used to evaluate STANAG Test 3A, the 0.50wt% rGO propellant mixture does not exceed the 4% Criteria Limit in the difference between the observed and calculated mass loss. Though the mixture passes the Test 3A criteria at the temperature of maximum derivative mass loss, knowing that the 4% limit is exceeded within the tested temperature range warrants further stability analysis.

STANAG 4147 Test 4: DSC

Test 4 is another test to understand the thermal stability of a propellant mixture is by analyzing any changes in exothermic behavior. This test evaluates incompatibility by comparing the peak value in the in the heat flow from the propellant admixture to the baseline. Fortunately, the SDT 2960 instrument used in this investigation simultaneously measures mass and heat flow from the sample during testing. To allow for direct comparison of each of the tested materials, the obtained heat flow values are divided by the initial mass of the sample to produce a specific heat flow (W/g). The specific heat flow curves for all the tested propellant mixtures are displayed in Figure 39.

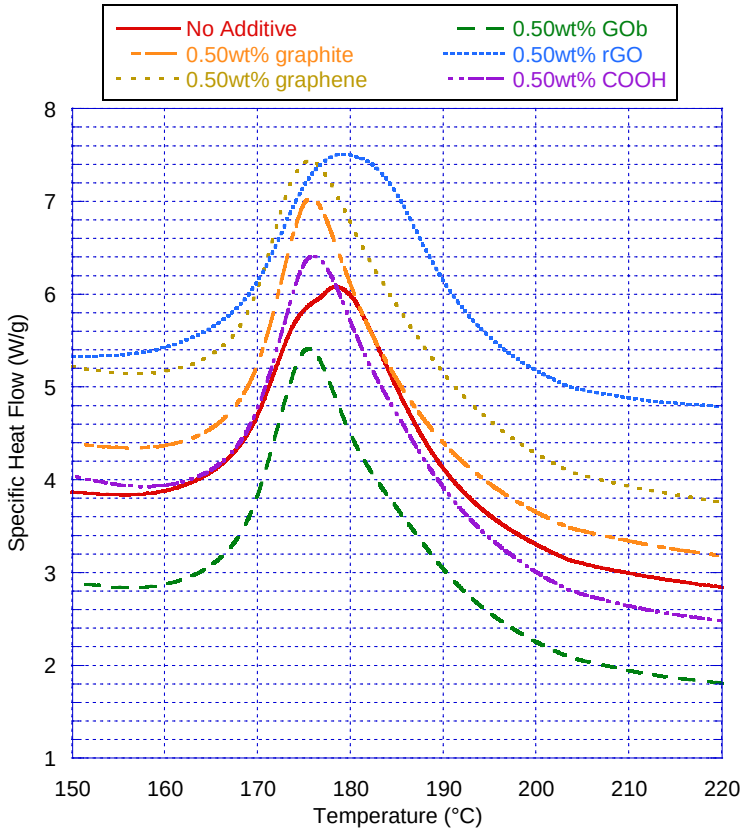

Figure 39: Differential Scanning Calorimetry (DSC) of Propellant Mixtures

As mentioned in a previous section, the peak value in specific heat flow from the samples for the majority of the additive materials, except GOb, is greater than that of the baseline; suggesting the additive material lead to a greater rate of heat release during propellant decomposition. A qualitative observation about the curves in Figure 39 is that the width of the peaks is relatively uniform for all the tested materials. This would suggest that the heat release is occurring across a similar temperature span, or indicate similar heat release and decomposition mechanisms are experienced by the mixtures. Also evident from visual inspection, these additive materials exhibit a slight shift in the temperature at which the peak value for heat flow occurs to cooler (lower) values. The Test 4 criteria states that for mixture components to be considered compatible, the temperature of the peak heat flux cannot shifted by more than 4°C cooler than the baseline propellant. Using the values presented in Table 8, the temperature of the peak heat flux

for the propellant admixtures can be subtracted by the baseline DB propellant. In this context, a mixture that exhibits a shift less than -4°C indicates some degree of incompatibility. The calculated temperature shifts are displayed in Table 9.

Table 9: Shift in Temperature of Peak Heat Flow

Material	Temperature of Peak Heat Flow (°C)	ΔT (°C)
0.50wt% graphite	175.6	-3.1
0.50wt% graphene	175.7	-3.0
0.50wt% GOb	175.6	-3.5
0.50wt% rGO	174.3	0.2
0.50wt% Carboxyl FGS	176.2	-2.6

Similar to the results of Test 3A in Table 8, each additive material propellant mixture satisfies the test criteria and has a shift that is less than the -4°C criteria. The difference is that the shift in peak heat flow temperature is more uniform than the shift in percent mass loss difference. This may indicate differences between the behavior of the decomposition of the individual powders compared to the thermal behavior of introducing carbon materials into the propellant. With the calculation and evaluation done with the DSC data collected, it can be confidently stated that the tested propellant admixtures pass the criteria of STANAG 4147 Test 4 for chemical compatibility.

Economic Impact

Apart from comparison of just linear burning rate or mass burning rate of each of the additive materials and concentration, the cost of the propellant mixture should be considered. Even with graphene materials becoming more available and cost effective, the price per gram of some of the carbon powders is considerably more than that of the propellant itself. Table 10 displays an estimated, percentage increase in price to a propellant mixture for the various additive material and concentrations. This table is based off the cost per mass available for bulk quantity

orders for the companies purchased from in this investigation. As development of graphene and graphite materials continues to advance, it is likely that these materials may experience a lowering in cost in the future or better pricing may be available to individuals or companies that would be interested in very large orders (>10kg) of materials

Table 10: Estimated Cost Increase of Propellant for Various Additive Material and Concentration

Material	Estimated* percent cost increase of DB propellant mixtures			
	0.25wt%	0.50wt%	0.75wt%	1.00wt%
Graphite	0.33	0.67	1.00	1.33
Graphene	0.53	1.05	1.58	2.10
GO	26.5	52.9	79.4	106
rGO	1515	3024	4536	6048
Carboxyl FGS	151	302	454	605

Evident in Table 10, the functionalized graphene materials would significantly increase the price per mass of a mix of the DB propellant with even small concentrations of additive material. The FGS materials require specialized processes to develop and lead to much larger price per mass. If economics are a major limitation, it would be necessary for the enhancement to the performance of the DB propellant to be significant to justify the purchase and use of these materials. In more definite terms, 1.00wt% of rGO (the largest relative cost increase) would lead to the DB mixture to cost on the order of 200$/lb.

One of the interested uses for enhanced materials is their use as a controllable parameter to tailor the performance of an ammunition charge. A charge can be composed of pellets of various propellant mixtures; the variety of rates of burning and gas generation of the various propellants in the composition are selected for a desired projectile performance. If one of the more costly propellant mixes with additives are used as one of the components of a charge, the increase in the cost per charge would be less impacted. Estimates on cost influence on charges is

* Price of most used additive materials and propellant is proprietary information.

not available as the information is confidential (military applications) or proprietary (firearm applications).

Chapter 7

Summary and Conclusion

This investigation aimed to evaluate how the mixing of carbon additives affects the performance and material properties of a double-base propellant. Graphite, graphene and functionalized graphene materials (graphene oxide, reduced graphene oxide, carboxyl functionalized graphene sheets) were mixed with a representative double-base propellant at different concentrations (0.25. 0.50, 0.75 & 1.00 weight percent) to observe the effect of the additives on the burning rate of the propellant and sensitivity to additive concentration.

It was found that the production of small-scale batches in a non-specialized lab setting presents difficulties in developing propellant test strands that were truly uniform and consistent from batch to batch. This has led to relatively large variability and uncertainty in the analyzed results. Even with this consideration, the additive-propellant mixtures did not exhibit any harmful or obvious thermal instabilities or chemical compatibilities. This fact allowed for the handling of these materials, and suggests they may be appropriate for long-term storage and sensitivity analysis. Imagery of the admixtures and isolated particles using a scanning electron microscope revealed that the sonication and mixing processes yielded, overall, compositions with favorably small (<50μm) and well distributed particles.

With the use of an optical strand burner and digital camera, the burn surface regression of the propellant mixtures were measured and a burning rate calculated from the video data. The previous mention of relatively large uncertainties leads to the conclusion that most of the materials and concentrations tested do not demonstrate significantly different performance than the control material, double base with no additive. 0.50wt% Graphene Oxide (GOb) is the

exception, and demonstrates statistically significant increase in burning rate as compared to the DB baseline. This statement is based off the fact that error ranges of 0.50wt% GOb and the DB propellant with no additive do not overlap. Overall, the admixtures exhibited a higher average burning rate than that of the control. This would suggest that the addition of a carbon powder changes the fundamental characteristics of the propellant to promote combustion. These tests do not give indication as to which mechanism or mechanisms lead to the increased burning rates.

Using a specific gravity bottle, precise measurements of the strand densities were obtained. By comparing the measured values to the calculated theoretical density for each additive material and concentration, it can confidently be said that the extruded and dried strands produced through the lab-scale process contained few to no internal voids that would lead to biased and unreliable burning rate data. The DB baseline with no additive and the non-functionalized carbon additives (graphite and graphene) demonstrate average strand densities within 1% of the theoretical density values. The functionalized graphene materials (GOb, rGO and carboxyl FGS) exhibit average strand densities greater than the calculate theoretical values. For 1.00wt% GOb, 0.75wt% and 1.00wt% rGO, and 0.50wt%, 0.75wt% and 1.00wt% Carboxyl FGS, this increase is of statistical significance. The increase in density could be due to fine particles slipping into interstitial spaces within the DB matrix, or, potentially, the functionalized groups present some chemical attraction within the DB propellant that leads to greater density.

The normalization of the data by the multiplication of test burning rate by the respective strand density gives an interesting insight of the performance and sensitivity of each material. Mass burning rate gives a better indication of the rate of gas generation experienced by the tested admixtures. This normalization does portray trends in mass burning rate unique from both burning rate and density comparison. Four admixtures (0.50wt% graphite, 0.50wt% GOb, 0.50wt% and 1.00wt% rGO) demonstrate markedly increased mass burning rate compared to that of the DB baseline. 0.50wt% GOb exhibits the largest value in mass burning rate of all tested

additive materials and concentrations; however, this value cannot be said to be statistically significant compared to the DB with no additive as there is a small overlap between the error ranges of the two propellants. The materials that do demonstrate statistically significant increase in mass burning rate compared to the baseline are 0.50wt% and 1.00wt% rGO. These materials would benefit further investigate as the sample size is relatively low and not represented by multiple batches of material. The normalization to mass burning rate also demonstrated that two materials, 0.75wt% and 1.00wt% graphite, exhibit statistically significant decrease in mass burning rate as compared to DB propellant with no additive.

The results of the thermogravimetric analysis (TGA) reveal that the propellant mixes with 0.50wt% of each of the additives are as thermally stable as the DB propellant with no additive, as determined by Test 3A and 4 from NATO STANAG 4147. The relative mass curves also show signs that some of the additive materials (rGO) enhance the decomposition rate of the DB propellant. In addition to the greater mass loss, the 0.50wt% rGO propellant mixture also exhibited one of the highest values in peak specific heat flow. These two observations suggest that the rGO additive demonstrates some enhancement to the decomposition of the DB propellant.

Considering all three methods of evaluating the combustion behavior of the DB propellant with and without the additive materials and concentration used in this investigation, it can be said that the DB propellant mixture with 0.50wt% GOb has enhanced combustion over the DB baseline. There is evidence that this enhancement could be due to some degree of catalytic activity of the additive on the base propellant.

Some of the current, commercial applications of DB propellants are dependent on the propellants ability to supply controlled and stable combustion. The analysis in this thesis has shown there is strong potential for carbon additives to be used as a controllable variable in propellant mixtures to tailor produced propellants or charges to desired performance characteristics. From the data in this thesis, some materials, graphite and rGO, demonstrate

drastic changes in burning rate and mass burning rate at different levels of weight concentrations. These materials would not be recommended for use as a ‘tuning nob’ for tailoring propellant performance, as slight deviation in added material could lead to large changes in the behavior of the propellant.

Conversely, propellant mixes with GOb demonstrate relatively smooth and continuous changes in burning rate and mass burning rate with changes in weight concentrations. In addition to that, the observed concentrations of GOb in this investigation exhibits inhibited performance and significantly enhanced performance. The graphene oxide material analyzed in this thesis holds significant potential for future investigation including large-scale production.

Admixtures that exhibit lower burning rate and mass burning rate value would be of values to applications of maintaining a pressure profile for ballistics and projectiles. Admixtures that exhibit higher burning rate and mass burning rate values could be of value to enhancing the performance of existing system like rocketry. Alternatively, an enhanced propellant could achieve the same level of performance of a system with less material, which could work to lower costs in producing those systems or even increase safety with transport and storage.

Future Work

Continuation of the research and procedures laid out in this investigation would work to create greater certainty and confidence. The relatively large variability in data and error ranges depicted in comparison charts warrant additional testing. Understanding the relation between burning rate and pressure would be of great value for the characterizing propellant performance across a range of pressure environments; however, the variability in manufactured strands through the lab-scale process presents an obstacle in achieving this goal.

Further characterization of the propellant admixture properties would allow greater certainty into which change introduced by the additive materials contributes most the influences seen in the combustion behavior of the DB propellant. Continuing TGA tests at different temperature ramp rates will allow for an empirical calculation of the activation energy of each of the propellant admixtures. Obtaining values of the thermal diffusivity for the propellant mixtures would provide a better understanding of how thermal energy is transferred and stored. Both of these property values, activation energy and thermal diffusivity, would provide reference value in which to compare experimentally achieved results with any theoretically calculated results.

The additive materials and concentrations tested in this investigation should be subjected to rigorous sensitivity tests such as friction, electrostatic discharge and impact. The insensitivity to temperature exhibited in the collected thermogravimetric analysis is reassuring, but the propellant admixtures must be evaluated to ensure that no other aspect in material stability is compromised by the introduction of the additives. Commercial production and use of the materials used in this investigation is not recommended until their safety and stability have been fully qualified.

The methods and aim of this investigation should also be applied to other formulations of double base propellants with lower concentrations of nitroglycerine. The results from this investigation paired with other literature evaluating the use of carbon additives on the effect of nitrocellulose combustion behavior establish the extreme bounds of nitroglycerine content. It would be of great interest if the results obtained from this investigation and others lead to a more general understanding of the interaction between nitrocellulose, nitroglycerine and carbon additives in combustion or thermal decomposition settings.

This investigation only shows that there are significant effects to the combustion behavior of the used DB propellant by introducing carbon additive, but does not give much insight into the exact mechanisms that lead to these effects. Molecular dynamic simulations, much like those

utilized in referenced sources, would provide a better understanding of the fundamental interactions of the molecules within the admixture. There is evidence of enhanced activity but without understanding the additives' role in combustion at the molecular level, it cannot be said if this is driven by catalytic activity of the additive materials.

References

1. Royal Swedish Academy of Sciences, “Graphene: Scientific Background on the Nobel Prize in Physics 2010,” 2010.
2. Wujcik, E. K., Monty, C. N., “Nanotechnology for Implantable Sensors: Carbon Nanotubes and Graphene in Medicine,” *WIREs*, Vol. 5, No. 3, 2013, pp. 233-249.
3. Hass, J., R. Feng, T. Li, X. Li, Z. Zong, W. A. De Heer, P. N. First, E. H. Conrad, C. A. Jeffrey, and C. Berger. "Highly ordered graphene for two dimensional electronics." *Applied Physics Letters*, Vol. 89, No. 14, 2006, 143106.
4. Faugeras, C., Faugeras, B., Orlita, M., Potemski, M., Nair, R. R., Geim, A. K., "Thermal Conductivity of Graphene in Corbino Membrane Geometry". *ACS Nano*, Vol. 4, No. 4, 2010, pp.1889–1892.
5. Lee, C., Wei, X., Kysar, J. W., Hone, J., "Measurement of the Elastic Properties and Intrinsic Strength of Monolayer Graphene," *Science*, Vol. 321, No. 5887, 2008, pp. 385–8.
6. Oberg, E., Jones, F. D., Horton, H. L., Ryffel, H. H., “Properties, Treatment, and Testing of Materials,” *Machinery’s Handbook*, 25th ed., Industrial Press Inc., New York, 1996, pp. 364-580.
7. Glassman, I., Yetter, R., “Diffusion Flames,” *Combustion*, 4th Ed., Elsevier, Massachusetts, 2008, pp. 311-372.
8. Chen, X., Chen, B., “Macroscopic and Spectroscopic Investigations of the Adsorptions of Nitroaromatic Compounds on Graphene Oxide, Reduced Graphene Oxide, and Graphene Nanosheets,” *Environ. Sci. Technol.*, Vol. 46, 2015, pp. 6181-6189.
9. Zhang, C., Wen, Y., Xue, X. “Self-Enhanced Catalytic Activities of Functionalized Graphene Sheets in the Combustion of Nitromethane: Molecular Dynamic Simulations by Molecular Reactive Force Field,” *ACS Appl. Mater. Interfaces*, Vol. 6, 2014, pp. 12235-12244.
10. Giem, A. K., Novoselov, K. S., “The Rise of Graphene,” *Nature Materials*, Vol. 6, 2007, pp. 183-191.
11. Ooi, J. B., Ismail, H. M., Swamy, V., Wang, X., Swain, A. K., Rajanren, J. R., “Graphite Oxide Nanoparticles as a Diesel Fuel Additive for Cleaner Emissions and Lower Fuel Consumption,” *Energy Fuels*, 2016.
12. Sabourin, J. L., Dabbs, D. M., Yetter, R. A., Dryer, F. L., and Aksay I. A., “Functionalized Graphene Sheet Colloids for Enhanced Fuel/Propellant Combustion.” *ACS Nano*, Vol. 3, No. 12, 2009, pp. 3945-3954.
13. Boyars, C., Klager, K., “Manufacture of Cast Double Base Propellants”, *Propellants Manufacture, Hazards, and Testing*, American Chemical Society, Washington D.C., 1969, pp. 1-28.
14. Kubota, N., “Combustion of Double Base Propellants,” *Propellants and Explosives*, Wiley-VCH, Weinheim, 2007, pp. 143-177.

15. MIL-G-155A, “Military Specification: Dry Graphite for Use in Ammunition,” Department of Defense, 1944.
16. Navalon, S. *et al.*; “Carbocatalysis by Graphene-Based Materials,” *Chemical Reviews*, Vol. 114, No. 12, 2014, pp. 6179−6212.
17. rGO synthesis, illustration, “https://www.utu.fi/en/units/sci/units/chemistry/research/mcca/PublishingImages/GO%20rGO.jpg”.
18. Liu, L. M. *et al.*, “Enhanced Thermal Decomposition of Nitromethane on Functionalized Graphene Sheets: Ab Initio Molecular Dynamics Simulations,” *Journal of the American Chemical Society*, Vol. 134, No. 6, 2012, pp. 19011−19016.
19. MIL-STD-652D (AR). “Miltary Standard Propellants, Solid for Cannons Requirements and Packing,” United States Army, 1990.
20. Bracuti, A. J., Bottei, L. A., Davis, R., “Potential Multipurpose Additives: Flash-erosion Suppressant,” ARRADCOM, LCWSL, 1983.
21. Agrawal, J. P., *High energy materials (propellants, explosives and pyrotechnics),* Wiley-VCH Verlag GmbH & Co. KGaA, Weinheim, 2010, p. 176.
22. Freedman, F., “BLAKE- A Thermodynamics Code Based on TIGER,” Army Research Laboratory, ARL-CR-422, 1998.
23. Kotlar, A. J., Birk, A., “In-bore Liquid Injection for Barrel Cooling: Comparison of Liquid and Solid Additives Using Constant Breach Pressure Ideal Gun Calculations,” Army Research Laboratory, ARL-TR-1915, 1999.
24. Jessup, R. R., Prosen, E. J., “Heats of Combustion and Formation of Cellulose and Nitrocellulose (Cellulose Nitrate),” *J. Res. Nat. Bureau of Standards*, Vol. 44, 1950, pp. 387-393.
25. Cox, J. D., Pilcher, G., “Thermochemistry of Organic and Organometallic Compounds,” Academic Press, London, 1970.
26. Carter, R. E., Warren, R. C, “Extrusion Stresses, Die Swell, and Viscous Heating Effects in Double Base Propellants,” *J. Rheol.*, Vol. 31, No. 2, 1987, pp. 151-173.
27. Kuo, K. K., Zhang, B. “Transient Burning Characteristics of JA2 Propellant Using Experimentally Determined Zel’dovich Map,” *J. Propulsion and Power*, Vol. 22, No. 2, 2006, pp. 455-461.
28. NATO STANNAG 4147 (Ed. 2), “Chemical Compatibility of Ammunition Components with Explosives (Non-Nuclear Applications),” NATO/PfP, 2001.
29. TA Instruments Inc., *SDT 2960: Operator’s Manual,* New Castle, DE, 2000, pp. 1-11 to 1-14.
30. Fiamengo, I., Sućeska M., Matečić Mušanić, S., “Determination of Nitroglycerine Content in Double Base Propellants by Isothermal Thermogravimetry,” *Central European Journal of Energetic Materials*, Vol. 7, No. 1, 2010, pp. 3-19.
31. ASTM D1429-13 Standard Test Methods for Specific Gravity of Water and Brine, ASTM International, West Conshohocken, PA, 2013.
32. Zhang, X., Hikal, W. M., Zhang, Y., Bhattacharia, S. K., Li, L., Panditrao, S., Wang, S., Weeks, B. L., “Direct Laser Initiation and Imporoved Thermal Stability

of Nitrocellulose/Graphene Oxide Nanocomposits," *Appl. Phys. Lett*. Vol. 102, No. 141905, 2013, pp. 1-4.

33. Dean, R. B., Dixon, W. J., "Simplified Statistics of Small Numbers of Observations," *Anal. Chem*, Vol. 23, No. 4, 1951, pp. 636-638.
34. Kanji, G. K., *100 Statistical Tests*, SAGE Publication Ltd., London, 1993.
35. Grubbs, F. E., "Procedures for Detecting Outlying Observations in Samples," *Technometrics*, Vol. 11, No. 1, 1969, pp. 1-21.
36. Miller, M. S., Anderson, W. R., "CYCLOPS, a Breakthrough Code to Predict Solid-Propellant Burning Rates," Army Research Laboratory, ARL-TR-2910, 2003.

Appendix A

Chemical Equilibrium Analysis

```
problem
        uv    rho,g/cc=0.2,   t,k=3800
react
```

Table 11: Thermodynamic Properties and Composition of Modeled Species

Name	T,k (K)	h (kJ/mol)	C	H	N	O
NG[24]	298	-370.7	3	5	3	9
NC (IIC)[25]	298	-685.69	6	7.0006	2.9994	10.9987
graphite	298	Available in CEA chemical library				
graphene	298	769.95	53	19		
grapheneO	298	469.69	53	19		4
grapheneOH	298	3.76	53	19		4
grapheneCOOH	298	-373.48	57	19		8
graphene_3.5nm	298	2312.53	185	43		
graphene_7nm	298	4407.49	361	75		
graphene_14nm	298	8695.9	713	139		

Table 12: Relative Weight Percentage Values Used for CEA calculations

Material	Relative Weight Percentage				
NG	41.00	40.8975	40.795	40.6925	40.59
NC	59.00	58.8525	58.705	58.5575	58.41
Additive	0.00	0.25	0.50	0.75	1.00

Appendix B

Extrusion Die Design

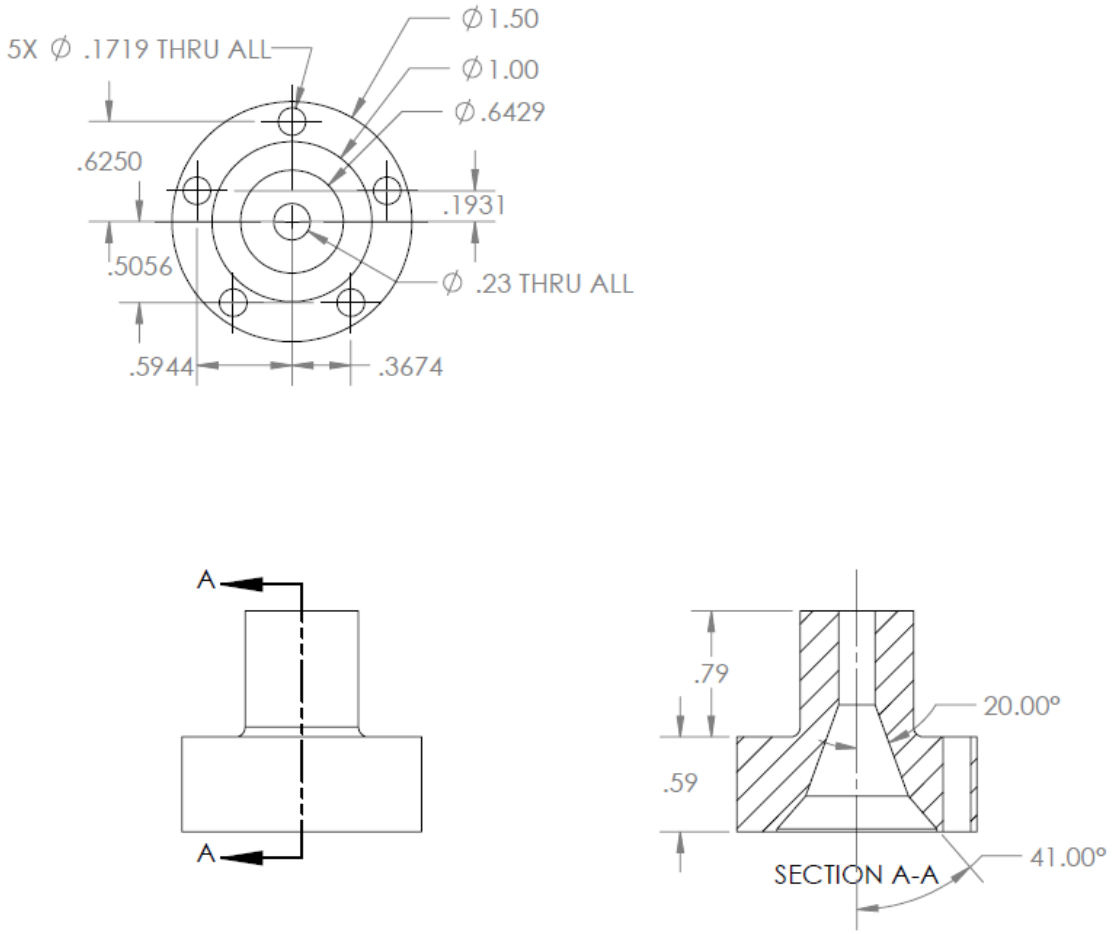

Figure 40: Mechanical Drawing of Extruder Die

All dimensions are in inches.

Appendix C

Regression Analysis Code

```
close all
clear all
clc
more off

%% Determine the path to data files-->Select either .TXT file (file name not used)
[FileName,PathName] = uigetfile(File Location);

%% Test & Evaluation parameters
fps=120.09;%frames per second of video
%scale= 6.28/139;%mm/px, scale of video [before 9/22/2016]
scale= 6.28/80;%mm/px, scale of video [calibrated: 9/22/2016]

%% Files Names for each data stream
Ext_Control_file = 'Ch1_Vin+.TXT';
Pressure_file = 'Ch4_Vin+.TXT';
%regress_abs_file= 'ImageJ_regression.txt';
regress_file= 'ImageJ_regression.txt';
%Ext_Control_file = 'Ch4_Vin+.TXT';
%Pressure_file = 'Ch1_Vin+.TXT';

%% load data files
Ext_Control = importdata([PathName Ext_Control_file],' ' ,27);
Pressure_temp = importdata([PathName Pressure_file],' ' ,27);
%regress_abs_temp = importdata([PathName regress_abs_file],'\t',1);
regress_temp = importdata([PathName regress_file],'\t',1);

%%Burning rate analysis from processed video
%regress_abs = regress_temp.data(:,:); Used for absolute time comparison
regress = regress_temp.data(:,:);
%regress(:,1)= relative slice #
%regress(:,2)= x location of cursor, not used in this analysis (pixel)
%regress(:,3)= y location of cursor, tracks regression (pixel)
%regress(:,4)= absolute slice #

regress(:,3)= regress(:,3)*scale;%space transformation (mm)
regress(:,4)= (regress(:,4)-1)/fps;%time transformation (s)
rdot= polyfit(regress(:,4),regress(:,3),1);
r_dot=rdot(1)%mm/s

%Uncertainty Analysis
By=4*scale;%mm, uncertainty in spatial measurment
Bt=1/fps;%s, uncertainty in temporal measurment
B_rdot= sqrt(2*(1/(regress(end,4)-regress(1,4)))^2 *By^2 +(((regress(end,3)-
regress(1,3))/((regress(end,4)-regress(1,4))^2))^2)*Bt^2)

abs_time= 0:.001:.001*length(Ext_Control.data);

for i = 1:size(Ext_Control.data)
    if Ext_Control.data(i) >= 2.5
        i_rel = i;
        break
    end
end
clear i
%Generate Relative Time by Shifting Abs. Time (Time = 0 when triggered)
rel_time = abs_time - abs_time(i_rel);

%% Time over which to average the pressure based on video of strand burning

time_start= rel_time(i_rel);
time_end= rel_time(i_rel)+ max(regress(1,4),regress(end,4));
```

```
        for i = 1:length(rel_time)
            if rel_time(i) >= time_start
                i_start = i;
                break
            end
        end
        clear i

        for i = i_start:length(rel_time)
            if rel_time(i) >= time_end
                i_end = i;
                break
            end
        end
        clear i

        %% Create pressure array over desired time range
        pressure = Pressure_temp.data(i_start:i_end);%was (i_start+i_rel:i_end+i_rel)
        %% Apply pressure calibration to PT voltage (S/N and Date of Cal.)
        % FOR 10k PT!!
        slope = 1972.1; % Setra 208 1262342 (7/14/2016)
        intercept = -136.62;
        %pressure_abst = slope * pressure + intercept + 14.7; %psia
        pressure = slope * pressure + intercept + 14.7; %psia

        %Plot Burning rate v. time and Pressure v. time on one plot
        figure(4)
        [ax,r,P]=plotyy(regress(:,4),regress(:,3),rel_time(i_start:i_end),pressure);
        set (r,'linestyle','none','marker','o');
        set (ax(2),'ylim',[0 10000])
        hold on
        plot(regress(:,4),rdot(1)*regress(:,4)+rdot(2),'r--');
        xlabel(ax(1), 'Time [s]')
        ylabel(ax(1), 'Burn Distance [mm]')
        ylabel(ax(2), 'Pressure [psia]')

        %% Average pressure, median pressure, and standard deviation
        Avg_Pressure = mean(pressure)
        % Median_Pressure = median(pressure)
        Std_Pressure = std(pressure)

        %% Filter out electrical noise and rerun?
        display('Look at the pressure plot:')
        prompt = 'Enter 1 to remove pressure spikes and recalculate or hit enter to
stop.';
        result = input(prompt);
        if size(result,1) > 0
            pressure(pressure > (Avg_Pressure+Std_Pressure)) = NaN;
            pressure(pressure < (Avg_Pressure-Std_Pressure)) = NaN;
            plot(rel_time(i_start+i_rel:i_end+i_rel),pressure,'r')
            pressure = pressure(~isnan(pressure));
            Avg_Pressure = mean(pressure)
        %     Median_Pressure = median(pressure)
            Std_Pressure = std(pressure)
        end
```